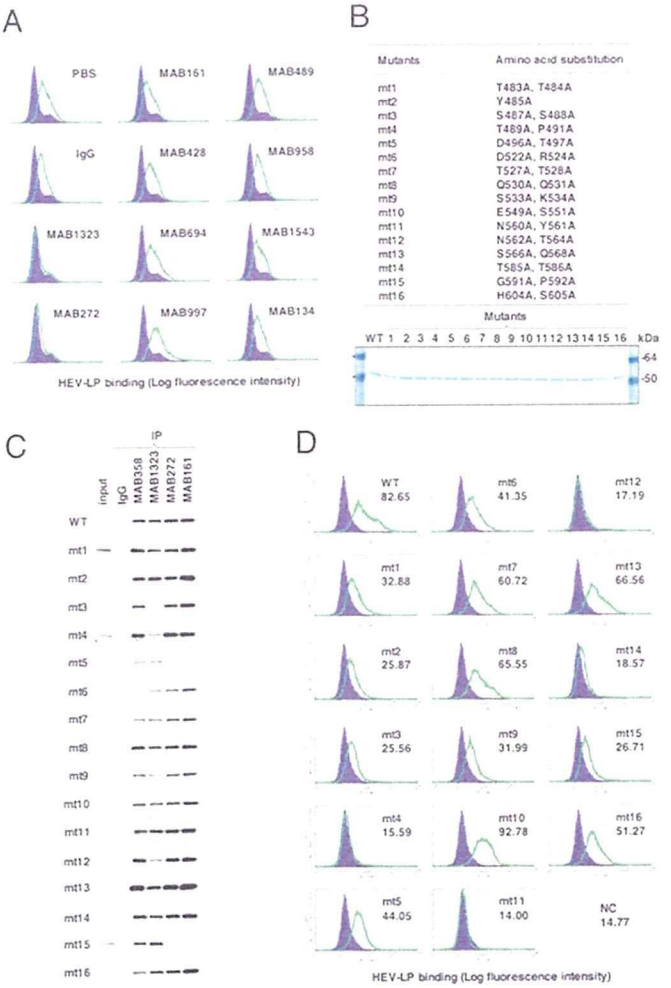

Fig. 3. Characterization of monoclonal antibodies and mutant HEV-LPs. (*A*) Neutralization of binding (NOB) of HEV-LP to Huh7 cells by monoclonal antibodies to HEV-LP. After preincubation of HEV-LP (10 μg/mL) with each of the monoclonal antibodies (20 μg/mL) for 1 h at 37°C, the mixture was inoculated into Huh7 cells and incubated for 1 h at 4°C. HEV-LP (lined area) bound to cells was detected by flow cytometry. The filled area indicates mock-incubated cells. (*B*) Construction of HEV-LP mutants. Sixteen HEV-LP mutants, in which the surface amino acid residues of the P domain were substituted, were constructed. The protein bands of 100 ng each of the purified wild-type and mutant HEV-LPs were visualized by Coomassie brilliant blue staining after SDS/PAGE. (*C*) Reactivities of NOB antibodies with the mutant HEV-LPs. Immunoprecipitation analyses of a series of HEV-LPs by NOB (MAB1323 and MAB272) or non-NOB antibodies (MAB358 and MAB161). Immunoprecipitated HEV-LPs were detected by an anti-HEV capsid rabbit polyclonal antibody. (*D*) Binding capability of the mutant HEV-LPs to Huh7 cells. Wild-type or mutant HEV-LPs (10 μg/mL) were incubated with Huh7 cells for 1 h at 4°C, and then HEV-LP (lined area) bound to cells was detected by flow cytometry. The filled area indicates mock-incubated cells. The MFI is shown in each panel.

domain of HEV-LP might also be involved in the cell binding. To examine this possibility, we prepared 16 HEV-LP mutants in which 1 or 2 amino acid residues at the surface of the P domain were substituted (Fig. 3*B*). The density fractionation assay indicated that all of the mutant proteins formed HEV-LP in the manner of the wild-type capsid protein. MAB358, which recognized an epitope on the M domain (Fig. S4), was capable of precipitating all of the mutants (Fig. 3*C*). MAB1323 exhibited no interaction with mt3 and a weak precipitation of mt4 and mt12. Both MAB272 and MAB161 exhibited no or weak precipitation of mt5 and mt15, whereas MAB272 but not MAB161 exhibited

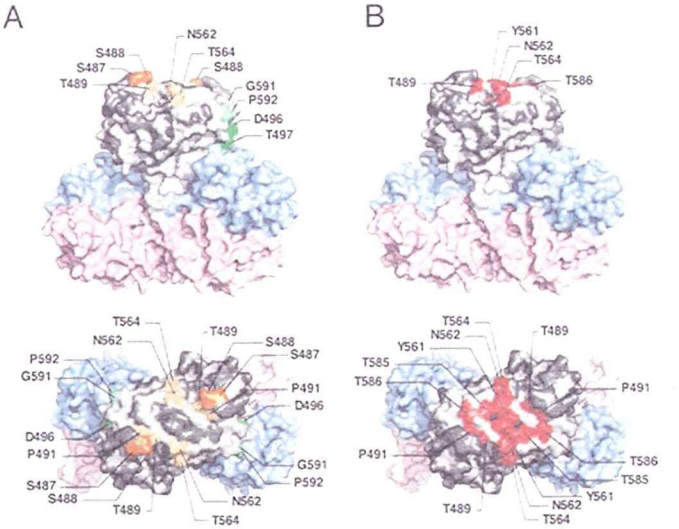

Fig. 4. Amino acid residues involved in the recognition by NOB antibodies and in the binding to Huh7 cells. Surface diagrams of the capsid protein dimer from a lateral (*Upper*) or top (*Lower*) view. (*A*) Amino acids in HEV-LP involved in the complete loss (deep color) or reduction (light color) of reactivity to MAB1323 and MAB272 are shown in orange and green, respectively. (*B*) Amino acids in HEV-LP responsible for binding to Huh7 cells are shown in red. Domains S, M, and P are colored pink, blue and gray, respectively. The substitutions in the P domain of HEV-LP that exhibited no effect on the reactivity with NOB antibodies or the binding to Huh7 cells are shown in dark gray.

NOB of HEV-LP to Huh7 cells (Fig. 3*A* and *C*). The substituted amino acids of these mutants are illustrated in the 3D structure of the capsid dimer (Fig. 4*A*), and these results suggest that the NOB antibodies MAB1323 and MAB272 recognize the peripheral region of the apical surface (orange) and the horizontal region (green) of the P domain above the M domain at the 3-fold axis, respectively.

Three-Dimensional Mapping of a Region Crucial for Binding to the Target Cells. To determine the region important for binding to the cell surface, the mutant HEV-LPs substituted into the P domain were also used in the assay of binding to Huh7 cells (Fig. 3*D*). The wild-type HEV-LP bound to Huh7 cells with a geographic mean fluorescence intensity (MFI) of 82.65. Among the mutants examined, mt4, mt11, mt12, and mt14 exhibited significantly low MFI values of less than 20. Similar results were obtained using A549 cells (Fig. S6). The amino acid residues required for cell binding were mapped in the central flexible region of the apical surface as shown in Fig. 4*B* (red). This region is partially overlapped with epitopes of MAB1323 (Fig. 4*A*) and other neutralizing antibodies reported by Schofield et al. (16) as shown in Fig. S7. These results suggested that the apical center region of the P domain is involved in the association with not-yet-identified cellular receptor(s).

Discussion

The expression of the truncated HEV capsid protein (amino acids 112–608) in insect cells resulted in assembly of HEV-LP, which retains an antigenicity similar to that of the native HEV particles (26, 37). This particle with a $T = 1$ symmetry has a diameter of 270 Å, which is smaller than the 320-Å diameter of the native virion detected in the fecal specimens of patients (25). It has been reported that the interior cavity of HEV-LP is too small to accommodate a viral RNA of 7.8 kb in length (28) and that the particles show no evidence of nucleotide contents (26, 28). Therefore, native HEV particles are sug-

Table 1. Data collection and processing statistics for HEV-LP

Data collection	
Space group	$P2_12_12_1$
Cell dimensions	
a, *b*, *c*, Å	336.8, 349.4, 359.5
X-ray wavelength, Å	1.0000
Resolution, Å	50–3.55 (3.68–3.55)
R_{merge}*	0.131 (0.498)
$I/\sigma I$	9.8 (3.2)
Completeness, %	99.9 (99.8)
Redundancy	5.6 (5.2)
Refinement	
Resolution range, Å	20–3.56
No. reflections	494,466
R_{work}/R_{free}	30.5/30.9
No. atoms	
Protein	215,400
B factors	
Protein	94.9
rmsd	
Bond length, Å	0.009
Bond angle, °	1.355

Values in square brackets refer to the highest-resolution shell.

*$R_{merge} = \Sigma_{hkl}\Sigma_i|I(hkl)_i - \langle I(hkl)\rangle|/\Sigma_{hkl}I(hkl)$, where $I(hkl)_i$ is the *i*th measurement of the intensity of reflection hkl and $\langle I(hkl)\rangle$ is the mean intensity of reflection *hkl*.

gested to be composed of a larger number and/or a larger size of capsid proteins than HEV-LP. In some cases of plant viruses with a $T = 3$ symmetry, the capsid proteins assembled into particles with a $T = 1$ symmetry by deletion of the N-terminal basic region (38, 39) or amino acid substitutions either in the N-terminal region or in the linker domain between the N-terminal region and S domain (39), suggesting that the N-terminal basic region plays an important role in switching of the transition from $T = 3$ to $T = 1$ symmetry. In addition, expression of the NV capsid protein in insect cells resulted in production of not only $T = 3$ large particles but also small particles thought to have the $T = 1$ symmetry (40). Based on many similarities of the capsid structures and their packaging of structurally related viruses, the native HEV particles are suggested to possess a $T = 3$ surface lattice. The flexibility of the proline-rich hinge linking the M and P domains could allow the capsid protein dimer to switch conformations between the A/B and C/C subunits found in $T = 3$ viruses. Although structure of the native HEV may be slightly different from that of the HEV-LP, the data obtained in this study by using HEV-LP should provide useful information to understand the structure of viral particle, life cycle, and pathogenesis of HEV. The S domain shares the jellyroll fold with some other icosahedral viruses (29–33). It was found that the capsid proteins with substitutions of Tyr-288 positioned at the center of the pentamer structure built in interS domain-interaction failed to assemble into HEV-LP. Alignment analysis of amino acid sequences using data available in GeneBank showed that Tyr-288 is completely conserved within 5 genotypes of HEV. Furthermore, residues corresponding to Tyr-288 of the HEV capsid protein are found in the structures of rNV (Phe-118), SMSV (Tyr-330), and CARMV (Phe-145), although the positions of these aromatic residues are different. Tyr-288 of HEV and Tyr-330 of SMSV located in the H-I loop and Phe-110 of rNV in the D–E loop are exposed at the outside surface of the particles, whereas Phe-145 of CARMV located in the D–E loop is exposed at the interior of the particle. These data suggest that the aromatic side chains of these residues are involved in hydrophobic interactions with those of the next subunits, assuring stable assembly of the particles. During entry into cells, rearrangement of the virion structure is required for release of the genome from the shell. However, the entry and uncoating mechanisms of HEV remain unknown. Because the center of the pentamer is the thinnest region of the particle and takes a channel-like structure (28), this region might also be important for uncoating and release of the viral RNA. It has been proposed that the 5-fold axis of poliovirus is involved in the genomic RNA translocation via conformational change of the virion initiated by binding to the receptor molecules (41, 42).

The first step in viral entry into a target cell is binding to the cellular receptors. The human hepatoma PLC/PRF/5 and lung epithelial A549 cell lines, which are highly susceptible to persistent HEV-infection (24), are likely to express functional HEV receptors on the cell surface. However, HEV-LP had reduced binding to these cells compared to the other cell lines examined. Therefore, the human hepatoma cell line Huh7, which also exhibited a susceptibility to HEV infection (13, 18) and readily bound to HEV-LP, was mainly used in this study. It has been reported that the P domains of noroviruses and the feline calicivirus were involved in the binding to the putative receptors, histo-blood antigens (35, 36) and the feline junctional adhesion molecule (34), respectively. The peptide of the HEV capsid protein (amino acids 368–606), which consists of a part of the M and an entire P domain, was shown to be capable of binding to several cell lines (13), suggesting that the P domain of HEV is also involved in the binding to the cell receptors. Indeed, the mutational analyses in this study indicated that the central flexible region of the top of the P domain of HEV-LP plays a crucial role for binding to Huh7 and A549 cells. This is consistent with a recent study by Graff et al. in which an N562Q mutant of HEV lost infectivity to culture cells and rhesus macaques despite the production of viral particles (18). Interestingly, a possible *N*-glycosylation site, Asn-562-Thr-Thr, is mapped in this region. *N*-glycosylation is an unusual posttranslational modification for nonenveloped viruses, except for rotaviruses (43). The mutant capsid mt12, which has substitutions of Asn-562 and Thr-564 to alanine, exhibited the same migration as the wild-type protein in SDS/PAGE, suggesting that the HEV-LP produced in insect cells was not glycosylated at Asn-562. Lack of *N*-glycosylation in the capsid protein has also been reported in mammalian cells infected with HEV (18), whereas some portion of the capsid protein was glycosylated and transported to the cell surface upon overexpression in mammalian cells (19). *N*-glycosylation of the HEV capsid at Asn-562 may have a negative effect on the receptor-binding, whereas it may play a positive role in other functions, including pathogenesis. The biological significance of the glycosylation of HEV capsid protein remains to be studied.

Although there is currently a lack of sensitive and reliable assays to determine the neutralizing activity of anti-HEV antibodies, the assay of NOB of HEV-LP binding to the target cells is thought to be a suitable alternative method. Measurement of the reactivity of a panel of mutant HEV-LPs revealed that the epitopes of MAB1323 and MAB272 antibodies are mapped in the peripheral region of the apical surface and the horizontal region of the P domain dimer, respectively. These results further support the notion that the P domain of HEV-LP is important for the binding to cells. MAB1323 is suggested to directly inhibit the interaction between HEV-LP and cellular receptors through binding to the apical surface, whereas MAB272 may have an allosteric effect, inducing conformational change of the P domain through binding to the horizontal region. A number of monoclonal antibodies are capable of neutralizing in vitro and in vivo infection of HEV (12–17), and many of them recognize conformational epitopes

of the capsid protein, as seen in the MAB1323 and MAB272 antibodies prepared in this study. Monoclonal antibodies against linear epitopes located in amino acids 578–607 of a genotype 1 capsid protein (16) were overlapped with a part of the putative receptor-binding domain and the epitope of MAB272, supporting the data of the present study. On the other hand, monoclonal antibodies against the linear epitopes located in amino acids 423–438 and amino acids 423–443 in the M domain of a genotype 1 capsid protein neutralized binding of a peptide derived from the capsid protein to cells and HEV-infection (13), suggesting the importance of the M domain in the binding step.

In summary, we have determined the crystal structure of HEV-LP produced in insect cells and demonstrated its structural characteristics in comparison with the structurally related animal and plant viruses. This study will provide useful information for elucidation of the molecular mechanisms of HEV-life cycles and for the development of prophylactic and therapeutic measures for hepatitis E.

Materials and Methods

Expression, Purification, and Crystallization of HEV-LP. The recombinant baculovirus encoding the ORF2 of the HEV genotype 3, 2712 strain was expressed in insect cells. HEV-LP was purified as described previously (28) and crystallized by the hanging-drop vapor-diffusion method. Details are reported in *SI Materials and Methods*.

Data Collection and Phase Determination. x-ray diffraction data were collected at 100 K on beamlines BL17A at the Photon Factory (KEK). The statistics of X-ray diffraction data collection are summarized in Table 1. The solved 3D structure of HEV-LP was submitted to the Protein Data Bank under the PDB accession code of 2ZTN. Details are reported in *SI Materials and Methods*.

ACKNOWLEDGMENTS. We thank H. Murase for her secretarial work and the staff of SPring-8 BL44XU beamline and synchrotron beamline NW-17A of the Photon Factory, High Energy Accelerator Research Organization for their assistance with the data collection. This work was supported in part by grants-in-aid from the Research and Development Program for New Bio-industry Initiatives of Bio-oriented Technology Research Advancement Institution (BRAIN) and the Foundation for Research Collaboration Center on Emerging and Re-emerging Infections.

1. Panda SK, Thakral D, Rehman S (2007) Hepatitis E virus. *Rev Med Virol* 17:151–180.
2. Purcell RH, Emerson SU (2008) Hepatitis E: An emerging awareness of an old disease. *J Hepatol* 48:494–503.
3. Navaneethan U, Al Mohajer M, Shata MT (2008) Hepatitis E and pregnancy: Understanding the pathogenesis. *Liver Int* 28:1190–1199.
4. Meng XJ, *et al.* (1997) A novel virus in swine is closely related to the human hepatitis E virus. *Proc Natl Acad Sci USA* 94:9860–9865.
5. Sonoda H, *et al.* (2004) Prevalence of hepatitis E virus (HEV) Infection in wild boars and deer and genetic identification of a genotype 3 HEV from a boar in Japan. *J Clin Microbiol* 42:5371–5374.
6. Okamoto H (2007) Genetic variability and evolution of hepatitis E virus. *Virus Res* 127:216–228.
7. Li TC, *et al.* (2005) Hepatitis E virus transmission from wild boar meat. *Emerg Infect Dis* 11:1958–1960.
8. Yazaki Y, *et al.* (2003) Sporadic acute or fulminant hepatitis E in Hokkaido, Japan, may be food-borne, as suggested by the presence of hepatitis E virus in pig liver as food. *J Gen Virol* 84:2351–2357.
9. Tam AW, *et al.* (1991) Hepatitis E virus (HEV): Molecular cloning and sequencing of the full-length viral genome. *Virology* 185:120–131.
10. Matsubayashi K, *et al.* (2004) Transfusion-transmitted hepatitis E caused by apparently indigenous hepatitis E virus strain in Hokkaido, Japan. *Transfusion* 44:934–940.
11. Huang FF, *et al.* (2004) Determination and analysis of the complete genomic sequence of avian hepatitis E virus (avian HEV) and attempts to infect rhesus monkeys with avian HEV. *J Gen Virol* 85:1609–1618.
12. Emerson SU, *et al.* (2006) Putative neutralization epitopes and broad cross-genotype neutralization of Hepatitis E virus confirmed by a quantitative cell-culture assay. *J Gen Virol* 87:697–704.
13. He S, *et al.* (2008) Putative receptor-binding sites of hepatitis E virus. *J Gen Virol* 89:245–249.
14. Meng J, *et al.* (2001) Identification and characterization of the neutralization epitope(s) of the hepatitis E virus. *Virology* 288:203–211.
15. Takahashi M, *et al.* (2008) Production of monoclonal antibodies against hepatitis E virus capsid protein and evaluation of their neutralizing activity in a cell culture system. *Arch Virol* 153:657–666.
16. Schofield DJ, Glamann J, Emerson SU, Purcell RH (2000) Identification by phage display and characterization of two neutralizing chimpanzee monoclonal antibodies to the hepatitis E virus capsid protein. *J Virol* 74:5548–5555.
17. Schofield DJ, Purcell RH, Nguyen HT, Emerson SU (2003) Monoclonal antibodies that neutralize HEV recognize an antigenic site at the carboxyterminus of an ORF2 protein vaccine. *Vaccine* 22:257–267.
18. Graff J, *et al.* (2008) Mutations within potential glycosylation sites in the capsid protein of hepatitis E virus prevent the formation of infectious virus particles. *J Virol* 82:1185–1194.
19. Zafrullah M, Ozdener MH, Kumar R, Panda SK, Jameel S (1999) Mutational analysis of glycosylation, membrane translocation, and cell surface expression of the hepatitis E virus ORF2 protein. *J Virol* 73:4074–4082.
20. Huang R, *et al.* (1999) Cell culture of sporadic hepatitis E virus in China. *Clin Diagn Lab Immunol* 6:729–733.
21. Kazachkov Yu A, *et al.* (1992) Hepatitis E virus in cultivated cells. *Arch Virol* 127:399–402.
22. Meng J, Dubreuil P, Pillot J (1997) A new PCR-based seroneutralization assay in cell culture for diagnosis of hepatitis E. *J Clin Microbiol* 35:1373–1377.
23. Tam AW, *et al.* (1997) In vitro infection and replication of hepatitis E virus in primary cynomolgus macaque hepatocytes. *Virology* 238:94–102.
24. Tanaka T, Takahashi M, Kusano E, Okamoto H (2007) Development and evaluation of an efficient cell-culture system for Hepatitis E virus. *J Gen Virol* 88:903–911.
25. Bradley D, *et al.* (1988) Aetiological agent of enterically transmitted non-A, non-B hepatitis. *J Gen Virol* 69:731–738.
26. Li TC, *et al.* (1997) Expression and self-assembly of empty virus-like particles of hepatitis E virus. *J Virol* 71:7207–7213.
27. Li TC, *et al.* (2005) Essential elements of the capsid protein for self-assembly into empty virus-like particles of hepatitis E virus. *J Virol* 79:12999–13006.
28. Xing L, *et al.* (1999) Recombinant hepatitis E capsid protein self-assembles into a dual-domain T = 1 particle presenting native virus epitopes. *Virology* 265:35–45.
29. Prasad BV, *et al.* (1999) X-ray crystallographic structure of the Norwalk virus capsid. *Science* 286:287–290.
30. Chen R, Neill JD, Estes MK, Prasad BV (2006) X-ray structure of a native calicivirus: Structural insights into antigenic diversity and host specificity. *Proc Natl Acad Sci USA* 103:8048–8053.
31. Morgunova E, *et al.* (1994) The atomic structure of Carnation Mottle Virus capsid protein. *FEBS Lett* 338:267–271.
32. Hogle JM, Chow M, Filman DJ (1985) Three-dimensional structure of poliovirus at 2.9 A resolution. *Science* 229:1358–1365.
33. Tsao J, *et al.* (1991) The three-dimensional structure of canine parvovirus and its functional implications. *Science* 251:1456–1464.
34. Bhella D, Gatherer D, Chaudhry Y, Pink R, Goodfellow IG (2008) Structural insights into calicivirus attachment and uncoating. *J Virol* 82:8051–8058.
35. Bu W, *et al.* (2008) Structural basis for the receptor binding specificity of Norwalk virus. *J Virol* 82:5340–5347.
36. Choi JM, Hutson AM, Estes MK, Prasad BV (2008) Atomic resolution structural characterization of recognition of histo-blood group antigens by Norwalk virus. *Proc Natl Acad Sci USA* 105:9175–9180.
37. Li TC, *et al.* (2004) Protection of cynomolgus monkeys against HEV infection by oral administration of recombinant hepatitis E virus-like particles. *Vaccine* 22:370–377.
38. Hsu C, *et al.* (2006) Characterization of polymorphism displayed by the coat protein mutants of tomato bushy stunt virus. *Virology* 349:222–229.
39. Kakani K, Reade R, Katpally U, Smith T, Rochon D (2008) Induction of particle polymorphism by cucumber necrosis virus coat protein mutants in vivo. *J Virol* 82:1547–1557.
40. White LJ, Hardy ME, Estes MK (1997) Biochemical characterization of a smaller form of recombinant Norwalk virus capsids assembled in insect cells. *J Virol* 71:8066–8072.
41. Belnap DM, *et al.* (2000) Molecular tectonic model of virus structural transitions: The putative cell entry states of poliovirus. *J Virol* 74:1342–1354.
42. Bubeck D, Filman DJ, Hogle JM (2005) Cryo-electron microscopy reconstruction of a poliovirus-receptor-membrane complex. *Nat Struct Mol Biol* 12:615–618.
43. Jayaram H, Estes MK, Prasad BV (2004) Emerging themes in rotavirus cell entry, genome organization, transcription and replication. *Virus Res* 101:67–81.

JOURNAL OF VIROLOGY, Aug. 2009, p. 7959–7969
0022-538X/09/$08.00+0 doi:10.1128/JVI.00889-09

Vol. 83, No. 16

Human VAP-C Negatively Regulates Hepatitis C Virus Propagation▽

Hiroshi Kukihara,[1] Kohji Moriishi,[1] Shuhei Taguwa,[1] Hideki Tani,[1] Takayuki Abe,[1] Yoshio Mori,[1] Tetsuro Suzuki,[2] Takasuke Fukuhara,[1,3] Akinobu Taketomi,[3] Yoshihiko Maehara,[3] and Yoshiharu Matsuura[1]*

Department of Molecular Virology, Research Institute for Microbial Diseases, Osaka University, Osaka,[1] Department of Virology II, National Institute of Infectious Diseases, Tokyo,[2] and Department of Surgery and Science, Graduate School of Medical Sciences, Kyushu University, Fukuoka,[3] Japan

Received 3 May 2009/Accepted 2 June 2009

Human vesicle-associated membrane protein-associated protein (VAP) subtype A (VAP-A) and subtype B (VAP-B) are involved in the regulation of membrane trafficking, lipid transport and metabolism, and the unfolded protein response. VAP-A and VAP-B consist of the major sperm protein (MSP) domain, the coiled-coil motif, and the C-terminal transmembrane anchor and form homo- and heterodimers through the transmembrane domain. VAP-A and VAP-B interact with NS5B and NS5A of hepatitis C virus (HCV) through the MSP domain and the coiled-coil motif, respectively, and participate in the replication of HCV. VAP-C is a splicing variant of VAP-B consisting of the N-terminal half of the MSP domain of VAP-B followed by the subtype-specific frameshift sequences, and its biological function has not been well characterized. In this study, we have examined the biological functions of VAP-C in the propagation of HCV. VAP-C interacted with NS5B but not with VAP-A, VAP-B, or NS5A in immunoprecipitation analyses, and the expression of VAP-C inhibited the interaction of NS5B with VAP-A or VAP-B. Overexpression of VAP-C impaired the RNA replication of the HCV replicon and the propagation of the HCV JFH1 strain, whereas overexpression of VAP-A and VAP-B enhanced the replication. Furthermore, the expression of VAP-C was observed in various tissues, whereas it was barely detected in the liver. These results suggest that VAP-C acts as a negative regulator of HCV propagation and that the expression of VAP-C may participate in the determination of tissue tropism of HCV propagation.

Hepatitis C virus (HCV) is a major causative agent of chronic liver disease and thus a major public health problem, infecting at least 3% of the world population (47). HCV infection proceeds to the persistent stage in approximately 80% of patients, leading to the development of cirrhosis in 20% to 50% of patients, of whom approximately 5% eventually develop hepatocellular carcinoma (12). HCV encompasses a single-stranded positive-sense RNA genome of approximately 9.6 kb, which encodes a large precursor polyprotein comprising approximately 3,000 amino acids (26). The structural proteins are cleaved from the N-terminal one-fourth of the polyprotein by the host signal peptidase and signal peptide peptidase (23, 32, 33), resulting in the maturation of the capsid protein, two envelope proteins and viroporin p7. The NS2 protease cleaves after the carboxyl terminus, and then NS3 cleaves the appropriate downstream positions to produce NS4A, NS4B, NS5A, and NS5B (8, 42), all of which form the replication complex along with several host proteins (5, 21). NS5B is the RNA-dependent RNA polymerase, which is a main enzymatic component of the replication complex of HCV (3), while NS5A is a membrane-anchored zinc-binding phosphoprotein that appears to possess diverse functions, including the suppression of host defense and the regulation of the virus's replication (1, 4, 6, 41), although its biological function remains unclear.

* Corresponding author. Mailing address: Department of Molecular Virology, Research Institute for Microbial Diseases, Osaka University, 3-1, Yamadaoka, Suita, Osaka 565-0871, Japan. Phone: 81-6-6879-8340. Fax: 81-6-6879-8269. E-mail: matsuura@biken.osaka-u.ac.jp.

▽ Published ahead of print on 10 June 2009.

The NS5A protein has been shown to interact with several host proteins, including vesicle-associated membrane protein (VAMP)-associated protein (VAP) subtype A (VAP-A) (44) and subtype B (VAP-B) (9), FKBP8 (34), MyD88 (1), FBL2 (46), human butyrate-induced transcript 1 (hB-ind1) (40), and so on (25). VAP-A and VAP-B also bind to NS5B, although it remains unclear whether these interactions modulate HCV replication positively or negatively (9, 44). VAP-A and VAP-B have been shown to associate with the cytoplasmic face of the endoplasmic reticulum (ER) and the Golgi apparatus (38) and to consist of the major sperm protein (MSP) domain, the coiled-coil domain, and the transmembrane (TM) region, in that order (30, 39), as shown in Fig. 1A. VAP was originally reported as a protein binding to VAMP, which is a synaptic vesicle SNARE protein required for synaptic-vesicle fusion in the nematode *Aplysia californica*, and was designated the 33-kDa VAMP-associated protein, VAP-33 (39). Two mammalian homologues, VAP-A and VAP-B, were subsequently identified (30, 38). The transcription of VAP-A and VAP-B is ubiquitously detected in mammalian organs, including the heart, placenta, lung, liver, skeletal muscle, and pancreas (30), suggesting that VAP family proteins are involved in diverse cellular functions other than neurotransmitter release (30, 38, 49). Several VAP-interacting proteins share the FFAT motif (two phenylalanines in an acidic tract), which has the consensus amino acid sequence EFFDAXE, as determined by a comparison among oxysterol binding proteins (OSBPs), OSBP-related proteins (ORPs) (20), and the ceramide transport protein CERT (10, 19), contributing to the regulation of fatty acid metabolism. The interaction of VAP family proteins with

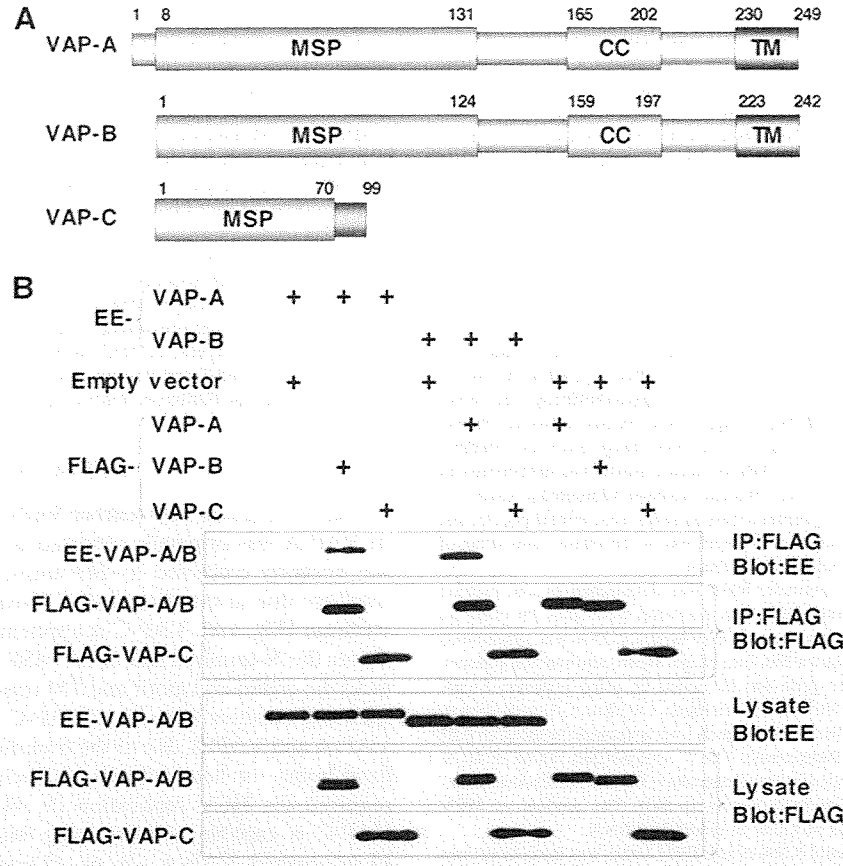

FIG. 1. VAP-C interacts with neither VAP-A nor VAP-B. (A) Structures of VAP family proteins. The MSP domain, the coiled-coil domain, and the TM region are indicated as MSP, CC, and TM, respectively. (B) Interaction among VAP family proteins. The expression plasmids encoding VAP proteins or empty vector (1 μg each) were transfected into 293T cells, FLAG-tagged VAP proteins coexpressed with EE-tagged VAP-A or VAP-B were immunoprecipitated (IP) with anti-FLAG antibody, and the resulting precipitates were examined by immunoblotting using anti-FLAG or anti-EE antibody. One percent of the volume of the lysate was used as an input control. The data in each panel are representative of the results of three independent experiments. +, present.

other host proteins, including VAMP and tubulin, is independent of the FFAT motif (16, 36, 38, 50). The third subtype of VAP is VAP-C, which is an alternative spliced isoform of VAP-B, consisting of the N-terminal half of the MSP domain and the subtype-specific 29 amino acids (Fig. 1A). However, its tissue distribution and physiological function remain largely unknown.

Glutathione *S*-transferase pulldown and immunoprecipitation analyses revealed that both VAP-A and VAP-B interact with NS5B and NS5A through the MSP domain and the coiled-coil domain, respectively (9, 44), and the MSP domains of VAP-A and VAP-B exhibit 82.3% homology. Although VAP-C possesses the N-terminal-half region of the MSP domain of VAP-B, the biological significance of VAP-C in the propagation of HCV has not yet been clarified. In this study, we examined the expression of VAP-C in human tissues and the effects of VAP-C expression on the RNA replication, translation, and particle formation of HCV.

MATERIALS AND METHODS

Cell lines. Cells of the human hepatoma cell line Huh-7, cell line Huh7OK1, and embryonic kidney cell line 293T were maintained in Dulbecco's modified Eagle's medium (DMEM) (Sigma, St. Louis, MO) containing 10% fetal calf serum (FCS) and nonessential amino acids (NEAA), while Huh 9-13 cells, which possess a subgenomic HCV RNA replicon of genotype 1b (21), were cultured in DMEM supplemented with 10% FCS, NEAA, and 1 mg/ml G418. The Huh7OK1 cell line exhibits the highest efficiency of propagation of strain JFH1 virus, as described previously (35). All cell lines were cultured at 37°C in a humidified atmosphere with 5% CO_2.

Antibodies. Chicken anti-human VAP-B antibody was described previously (9). Rabbit anti-human VAP-C antibody was prepared by immunization using synthetic peptides of the amino acid residues from 86 to 98, QPHFSISPNW EGR, which region does not share the homology to VAP-A and VAP-B. The mouse monoclonal antibody to human VAP-A was purchased from BD Pharmingen (San Diego, CA). Mouse monoclonal antibodies to influenza virus hemagglutinin (HA) and the GluGlu (EE) tag were from Covance (Richmond, CA). Mouse and rabbit anti-FLAG antibodies and mouse anti-β-actin monoclonal antibody were from Sigma. Rabbit polyclonal antibody to NS5A was prepared as described previously (34). Mouse anti-NS5A monoclonal antibody was from Austral Biologicals (San Ramon, CA).

Plasmids. A cDNA clone encoding NS5A was amplified from HCV genotype 1b strain J1 (9) (GenBank database accession number D89815) by PCR, using *Pfu* turbo DNA polymerase (Stratagene, La Jolla, CA). The fragments were then cloned into the appropriate sites in pEF-FLAG pGBK puro (13). The DNA fragment encoding NS5B of the J1 strain was generated by PCR and cloned into pCAGGs-PUR (31). The DNA fragment encoding human VAP-A was amplified by PCR from a human fetal-brain library (Clontech, Palo Alto, CA) and was introduced into pEF-FLAG pGBK puro and pEF-EE hygro (13), as described previously (9). A DNA fragment encoding VAP-C was amplified from cDNA of hepatoma cell line Huh-7 and was introduced into pEF-FLAG pGBK puro. Pro^{56}-to-Ser (P56S) mutants of VAPs were generated by site-directed mutagen-

esis (11). All PCR products were confirmed by sequencing with an ABI Prism 3130 genetic analyzer (Applied Biosystems, Tokyo, Japan).

Transfection, immunoblotting, and immunoprecipitation. Cells were seeded onto a six-well tissue culture plate 24 h before transfection. The plasmids were transfected into cells by liposome-mediated transfection using TransIT LT1 (Mirus Bio, Madison, WI). These transfected cells were harvested at 36 h posttransfection, washed three times with 1 ml of ice-cold phosphate-buffered saline (PBS), and suspended in 0.2 ml lysis buffer (20 mM Tris-HCl, pH 7.4, containing 135 mM NaCl and 1% Triton X-100) supplemented with protease inhibitor cocktail (Roche, Indianapolis, IN). The cell lysates were sonicated at 4°C for 5 min, incubated for 30 min at 4°C, and centrifuged at 15,000 rpm for 30 min at 4°C. The supernatant was subjected to immunoprecipitation analyses as described previously (27). The immunoprecipitated proteins were boiled in 30 μl of loading buffer and then subjected to sodium dodecyl sulfate–12.5% polyacrylamide gel electrophoresis. The proteins were transferred to polyvinylidene difluoride membranes (Millipore, Bedford, MA) and then reacted with primary antibody and secondary horseradish peroxidase-conjugated antibody. The immunocomplexes were visualized with Super Signal West Femto substrate (Pierce, Rockford, IL) and detected by using an LAS-3000 image analyzer (Fujifilm, Tokyo, Japan). The distribution of VAPs in human organs was determined by using premade human tissue lysates (Protein medleys; Clonetech), which are aliquots of various organ lysates prepared from samples from several people, and liver tissues obtained during surgery after approval of the ethical committee of Kyushu University Graduate School of Medicine.

Real-time PCR. The HCV genomic RNA was determined by the method described previously (40). Total RNA was prepared from cells by using an RNeasy mini kit (Qiagen, Tokyo, Japan). First-strand cDNA was synthesized using an RNA LA PCR kit (Takara Bio, Inc., Shiga, Japan) and random primers. Expression of the appropriate gene was estimated by using platinum SYBR green quantitative PCR SuperMix UDG (Invitrogen, Carlsbad, CA) according to the manufacturer's protocol. Fluorescent signals were estimated by using an ABI Prism 7000 system (Applied Biosystems). The 5′ untranslated region of HCV and the glyceraldehyde-3-phosphate dehydrogenase (GAPDH) mRNA were amplified using primer pairs described previously (40). The amount of HCV genomic RNA was normalized with that of GAPDH mRNA.

Focus-forming assay. The viral RNA of the JFH1 strain was introduced into the Huh7OK1 cell line according to the method of Zhong et al. (51). The culture supernatant was collected at 7 days posttransfection and used as the infectious HCV particles. Huh7OK1 cells in DMEM containing 10% FCS were seeded at 5×10^4 cells per well into a 24-well plate 12 h before infection. The cells were infected with the JFH1 strain at a multiplicity of infection (MOI) of 0.05 and incubated at 37°C for 2 h. The medium was replaced with fresh DMEM containing 10% FCS and NEAA at 2 h postinfection. The cells were fixed with 4% paraformaldehyde at 96 h postinfection and permeabilized with PBS containing 0.2% Triton X-100. These fixed and permeabilized cells were stained with the anti-NS5A mouse monoclonal antibody and Alexa Fluor (AF) 488-conjugated antibody to mouse immunoglobulin G (Molecular Probes, Eugene, OR). Clusters of infected cells stained with the NS5A antibody were derived from a single infectious focus, and virus titers were represented as focus-forming units/ml.

Quantification of the HCV core protein by ELISA. The HCV core protein was quantified by using an Ortho HCV antigen enzyme-linked immunosorbent assay (ELISA) test (Ortho Clinical Diagnostics, Tokyo, Japan) according to the manufacturer's instructions. To determine the intracellular expression of core protein, Huh7OK1 cells were infected with the infectious HCV particles described above, lysed with the lysis buffer on ice, and applied to the ELISA after 100- to 10,000-fold dilution with PBS. Total protein was quantified by using a Micro BCA protein assay reagent kit (Pierce). The intracellular and extracellular levels of expression of the core protein were normalized by the total amount of protein.

Effect of the VAP expression on the cap-independent translational activity of the viral IRES. The cDNA fragment encoding a firefly luciferase was excised from a pGL3 basic plasmid (Promega, Madison, WI) and introduced into the downstream region of the *Renilla* luciferase gene of pRL-CMV (cytomegalovirus) (Promega). Then, the cDNA fragments encoding the internal ribosome entry site (IRES) of the HCV strains Con1 and JFH1 were introduced between the *Renilla* and firefly luciferase genes, and the resulting plasmids were designated pRL-CMV-HCVCon1 and pRL-CMV-HCVJFH1, respectively (see Fig. 4A). The IRES region of HCV was replaced with that of poliovirus (PV) or encephalomyocarditis virus (EMCV), and the plasmids designated pRL-CMV-PV and pRL-CMV-EMCV, respectively (see Fig. 4B). Each reporter plasmid was introduced into Huh7OK1 cells that had been transfected with the expression plasmid encoding FLAG-green fluorescent protein (GFP), FLAG–VAP-A, FLAG–VAP-B, or FLAG–VAP-C 24 h previously, and cells were harvested at 48 h posttransfection. Luciferase activities in cells were measured by using a dual-luciferase reporter assay system (Promega). The activity of firefly luciferase was normalized with that of *Renilla* luciferase and represented as relative luciferase activity (RLU).

Indirect immunofluorescence assay. The Huh 9-13 cells were cultured on glass slides and transfected with the expression plasmids encoding FLAG-tagged VAPs, P56S VAP mutants, or empty vector. The resulting cells were fixed at 72 h posttransfection with 4% paraformaldehyde in PBS at room temperature for 30 min. After being washed twice with PBS, cells were permeabilized for 20 min at room temperature with PBS containing 0.25% saponin and blocked with PBS containing 1% bovine serum albumin (BSA-PBS) for 60 min at room temperature. The cells were then incubated with BSA-PBS containing rabbit anti-FLAG and mouse anti-NS5A antibodies at 37°C for 60 min, washed three times with PBS containing 1% Tween 20 (PBS-T), and incubated with BSA-PBS containing AF 488-conjugated goat anti-rabbit immunoglobulin G and AF 594-conjugated goat anti-mouse antibodies at 37°C for 60 min. Finally, the cells were washed three times with PBS-T and observed with a FluoView FV1000 laser-scanning confocal microscope (Olympus, Tokyo, Japan).

RESULTS

VAP-C interacts with neither VAP-A nor VAP-B. The length of VAP-A was originally reported to be 242 amino acids but was recently corrected to 249 amino acids in the GenBank database due to the detection of 7 extra amino acids in the N terminus (Fig. 1A). VAP-C is a splicing variant of VAP-B that shares the N-terminal half of the MSP domain with VAP-B but lacks the coiled-coil motif and TM region (Fig. 1A). The region spanning residues 71 to 99 of VAP-C exhibits no homology to VAP-A and VAP-B, due to the frameshift. VAP-A and VAP-B form homo- or heterodimers via their TM domains, which is required for HCV replication (9, 44). To examine whether VAP-C is capable of interacting with VAP-A and VAP-B, FLAG-tagged VAP-A, -B, or -C was coexpressed with EE-tagged VAP-A or -B in 293T cells and was immunoprecipitated with the anti-FLAG antibody. Although EE-tagged VAP-A and VAP-B were coprecipitated with FLAG-tagged VAP-B and VAP-A, as reported previously, FLAG–VAP-C was precipitated with neither EE–VAP-A nor EE–VAP-B (Fig. 1B). These results indicate that VAP-C does not interact with VAP-A and VAP-B.

VAP-C binds to NS5B and interrupts the interaction of VAP-A and VAP-B with NS5B. VAP-A and VAP-B were identified as NS5A-binding proteins by yeast two-hybrid screening (9, 44). The coiled-coil domains of VAP-A and VAP-B were involved in the binding to NS5A, contributing to the efficiency of HCV replication (9, 44). However, VAP-C does not have the coiled-coil domain (Fig. 1A) and, therefore, VAP-C was expected not to interact with NS5A. To examine whether or not interaction between VAP-C and NS5A actually occurred, HA-tagged NS5A was coexpressed with FLAG-tagged VAP-A, -B, or -C in 293T cells and was immunoprecipitated with anti-HA antibody (Fig. 2). The results showed that the expression level of FLAG–VAP-C in the transfected cells was comparable to that of FLAG–VAP-A or FLAG–VAP-B (Fig. 2A, left). Although FLAG-tagged VAP-A and VAP-B were coprecipitated with HA-NS5A, no precipitation of FLAG–VAP-C with NS5A was detected (Fig. 2A, right), indicating that VAP-C does not interact with NS5A.

The RNA-dependent RNA polymerase NS5B was shown to interact with VAP-A through the MSP domain (44). The region spanning residues 1 to 70 of VAP-C is the same as the N-terminal-half region of the MSP domain of VAP-B and exhibits 77% homology to that of VAP-A (Fig. 1A). To exam-

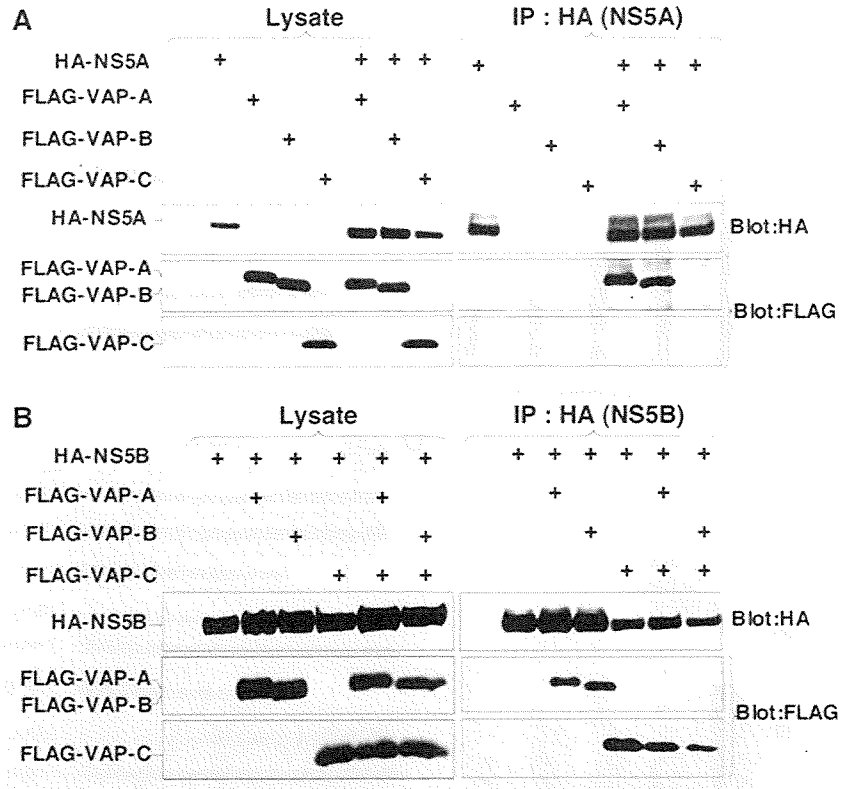

FIG. 2. VAP-C binds to NS5B but not NS5A and interrupts the interaction of VAP-A and VAP-B with NS5B. (A) The expression plasmids encoding NS5A or VAP proteins (1 μg each) were transfected into 293T cells after adjusting the total amounts of DNA to 2.0 μg with empty plasmid. HA-tagged NS5A was coexpressed with either FLAG-tagged VAP-A, VAP-B, or VAP-C in 293T cells and immunoprecipitated (IP) with anti-HA antibody, and the resulting precipitates were immunoblotted using anti-FLAG or anti-HA antibody. (B) The expression plasmids encoding NS5B or VAP proteins (1 μg each) were transfected into 293T cells after adjusting the total amounts of DNA to 3.0 μg with empty plasmid. HA-tagged NS5B was coexpressed with either FLAG-tagged VAP-A or VAP-B in the presence or absence of FLAG-tagged VAP-C in 293T cells and immunoprecipitated (IP) with anti-HA antibody, and the resulting precipitates were immunoblotted using anti-FLAG or anti-HA antibody. One percent of the lysate was used as an input control. The data in each panel are representative of the results of three independent experiments. +, present.

ine whether VAP-C is capable of interacting with NS5B, as are VAP-A and VAP-B, HA-NS5B was coexpressed with FLAG–VAP-A, FLAG–VAP-B, or FLAG–VAP-C in 293T cells and was immunoprecipitated with anti-HA antibody (Fig. 2B). Although substantial amounts of FLAG-tagged VAP-A, VAP-B, and VAP-C were coexpressed, and although all three were coprecipitated with HA-NS5B at comparable levels, the interaction of HA-NS5B with FLAG-tagged VAP-A or VAP-B was impaired by the coexpression of VAP-C, while FLAG–VAP-C was coprecipitated with HA-NS5B instead of FLAG-tagged VAP-A or VAP-B. These results suggest that VAP-C is capable of binding to NS5B and that the expression of VAP-C interrupts the interactions of NS5B with VAP-A and VAP-B.

Expression of VAP-C impairs the replication of HCV. VAP-A and VAP-B are known to support the replication of HCV RNA (2, 7). To examine the effect of VAP-C on the replication of HCV, FLAG–VAP-C was expressed in HCV replicon cells, Huh 9-13, in which a subgenomic HCV RNA of the genotype 1b strain Con1 was autonomously replicating. Huh 9-13 cells transfected with a plasmid encoding FLAG–VAP-C were harvested periodically up to 72 h posttransfection. The levels of replication of viral RNA and expression of NS5A were determined by real-time PCR and immunoblotting, respectively (Fig. 3). The expression of VAP-C reduced the intracellular RNA of the subgenomic HCV replicon in accordance with the incubation period after transfection with the expression plasmid of FLAG–VAP-C; the empty plasmid did not reduce the intracellular RNA (Fig. 3A). The expression of NS5A was gradually decreased and was undetectable at 72 h posttransfection, in contrast to the increase of VAP-C expression (Fig. 3B).

Next, to determine the effects of VAP-C expression on the replication of HCV, Huh 9-13 cells were transfected with 0 to 4 μg of the expression plasmid encoding VAP-A, VAP-B, or VAP-C and the replication of the subgenomic HCV RNA was determined at 48 h posttransfection. Although the HCV replicon cells transfected with 4 μg of a plasmid encoding FLAG–VAP-B exhibited enhancement of the RNA replication, those transfected with an equivalent amount of plasmid encoding FLAG–VAP-A or empty vector showed a slight reduction of HCV RNA replication. In contrast, the replicon cells transfected with a plasmid encoding FLAG–VAP-C exhibited a clear reduction of the HCV RNA replication in a dose-dependent manner (Fig. 3C). The expression of FLAG-tagged VAP-A, VAP-B, or VAP-C in the replicon cells was increased in correspondence with the amount of the transfected plasmid

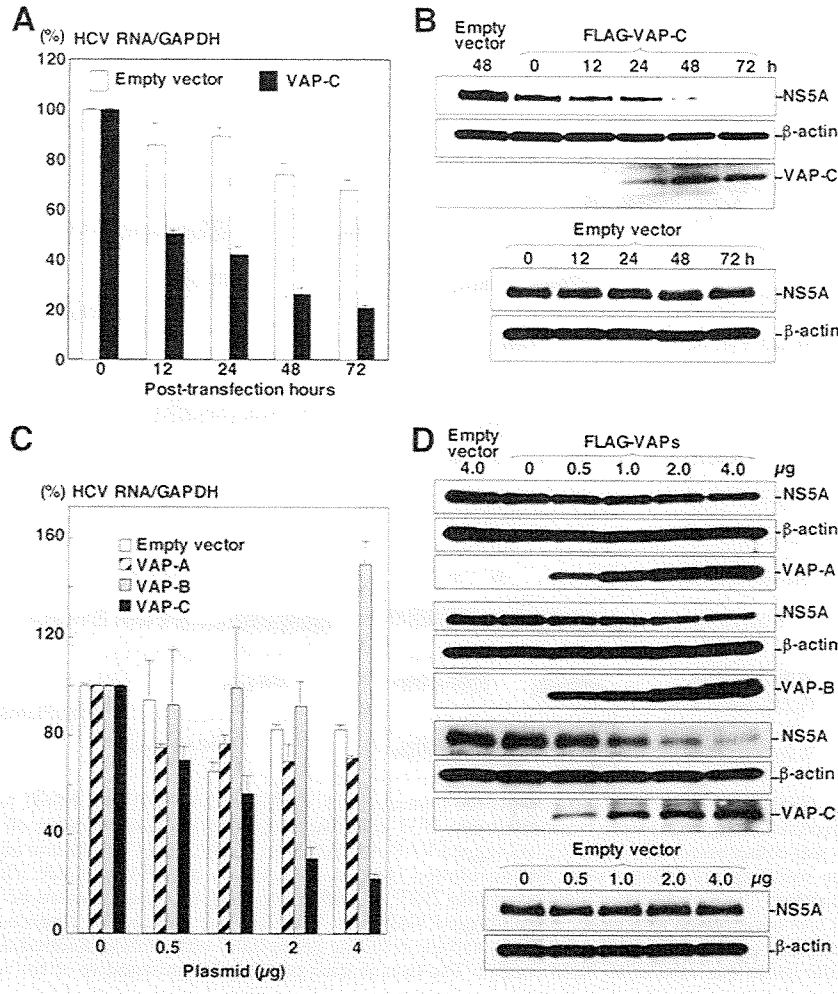

FIG. 3. Expression of VAP-C impairs the replication of HCV. (A) HCV replicon cells (Huh 9-13) were transfected with 4 μg of the expression plasmids encoding FLAG-tagged VAP-C or empty vector, and the level of intracellular HCV RNA was determined at 0, 12, 24, 48, or 72 h posttransfection by real-time PCR after normalization with GAPDH mRNA. The value of HCV RNA at 0 h posttransfection in the cell line transfected with the empty plasmid is represented as 100%. Data in this panel are shown as means ± standard deviations. (B) Huh 9-13 cells were transfected with 4 μg of the plasmid encoding FLAG-tagged VAP-C or empty plasmid, and the levels of expression of NS5A, β-actin, and VAP-C were determined at 0, 12, 24, 48, or 72 h posttransfection by immunoblotting using anti-NS5A, anti-β-actin, or anti-FLAG tag antibody. (C) Huh 9-13 cells were transfected with 0 to 4 μg of the plasmids encoding FLAG-tagged VAP-A, VAP-B, or VAP-C or empty vector, and the level of intracellular HCV RNA was determined at 72 h posttransfection as described for panel A. Data in this panel are shown as means ± standard deviations. (D) Huh 9-13 cells treated as described for panel C were harvested at 72 h posttransfection, and the levels of expression of NS5A, β-actin, VAP-A, VAP-B, and VAP-C were determined by immunoblotting. The data in each panel are representative of the results of three independent experiments.

(Fig. 3D), and the expression of NS5A was suppressed in accordance with the expression of FLAG–VAP-C, whereas the expression of FLAG–VAP-A and FLAG–VAP-B exhibited no effect on the expression of NS5A. These results suggest that the expression of VAP-C impairs the replication of HCV RNA.

VAP-C exhibits no effect on the IRES-dependent translation. The expression of VAP-C was shown to suppress the replication of the HCV RNA replication of the replicon cells. Next, to determine the effect of VAPs on the translation of HCV RNA, the reporter plasmid encoding the *Renilla* luciferase gene under the control of the CMV promoter and the firefly luciferase gene under the IRES of HCV, PV, or EMCV, in that order, was prepared as shown in Fig. 4. These reporter plasmids were introduced into Huh7OK1 cells 24 h after transfection of the expression plasmids encoding VAP-A, VAP-B, or VAP-C and harvested at 48 h posttransfection, and then the RLUs were determined. Although VAP-C exhibited a slight increase in the IRES-dependent translations of the HCV strains Con1 and JFH1, no significant effect of the expression of the VAPs on the HCV IRES-dependent translation was observed (Fig. 4A). Similarly, the expression of each of the VAPs in Huh7OK1 cells exhibited no significant effect on the IRES-dependent translation of PV or EMCV (Fig. 4B). These results indicate that the suppression of HCV RNA replication by the expression of

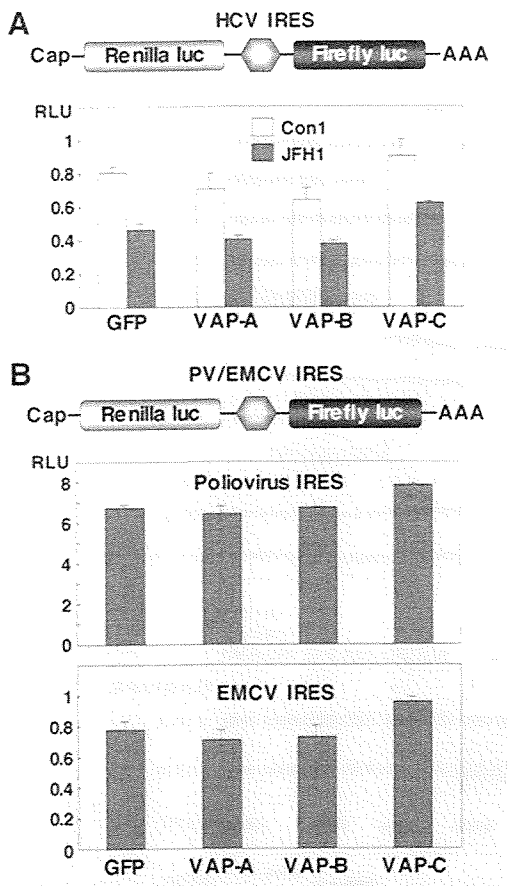

FIG. 4. VAP-C exhibits no effect on the viral IRES-dependent translation. (A) Top: structure of a reporter plasmid encoding the *Renilla* luciferase gene under the control of the CMV promoter and the firefly luciferase gene under the HCV IRES, in order. Bottom: the reporter plasmid was introduced into Huh7OK1 cells 24 h after transfection of the expression plasmids encoding VAP-A, VAP-B, or VAP-C, the cells harvested at 48 h posttransfection, and the RLUs determined after standardization with the expression of *Renilla* luciferase. (B) Top: structure of a reporter plasmid encoding the *Renilla* luciferase gene under the control of the CMV promoter and the firefly luciferase gene under the PV or EMCV IRES, in order. Bottom: each of the reporter plasmids was introduced into Huh7OK1 cells, and the RLU values were determined as described for panel A. Data in this figure are shown as the means ± standard deviations.

VAP-C was not due to the suppression of the IRES-dependent translation of the viral RNA genome.

VAP-C impairs HCV propagation. To examine the effect of VAP expression on HCV propagation, Huh7OK1 cells transfected with the expression plasmids encoding VAP-A, VAP-B, or VAP-C were infected with JFH1 virus, and the levels of production of the viral RNA, core protein, and infectious particles were determined at 96 h postinfection. The production of intracellular and extracellular viral RNA was increased up to 10 to 30 times and 2 to 3 times, respectively, by the expression of VAP-A or VAP-B whereas it was clearly decreased in a dose-dependent manner by the expression of VAP-C (Fig. 5A). Although the extracellular core protein was increased from 0.6 to 2.6 nmol/liter by the expression of VAP-A or VAP-B, as seen in the production of viral RNA, the intracellular core protein showed only a marginal increase (40 to 65 nmol/liter) (Fig. 5A). Although the reason for the discrepancy between the intracellular production of viral RNA and core protein is not known at the moment, some mechanisms other than RNA translation might be involved, because VAP expression exhibited no effect on the HCV IRES-dependent translation, as shown in Fig. 4A. In contrast to the enhancement of core protein production by the expression of VAP-A or VAP-B, the expression of VAP-C significantly reduced both the intracellular and extracellular expression of the core protein (Fig. 5A). Furthermore, the production of infectious particles in the culture supernatants of Huh7OK1 cells infected with JFH1 virus was slightly enhanced by the expression of VAP-A or VAP-B, whereas it was suppressed by the expression of VAP-C (Fig. 5A). To further confirm the effects of VAPs on the expression of HCV proteins, Huh7OK1 cells transfected with various amounts of the expression plasmids of VAP-A, VAP-B, or VAP-C and infected with the JFH1 virus were examined by immunoblotting (Fig. 5B). Although the expression of VAP-A or VAP-B exhibited no effect on NS5A expression, VAP-C expression clearly decreased the expression of NS5A in a dose-dependent manner. These results clearly indicate that the expression of VAP-C negatively regulates HCV propagation. Overexpression of VAP-C did not affect the endogenous expression of VAP-A or VAP-B (Fig. 5C), suggesting that suppression of HCV propagation by VAP-C is not due to the reduction of VAP-A or VAP-B expression.

Lack of VAP-C expression in human livers. VAP-C consists of the first 70 amino acid residues of VAP-B and the subtype-specific 29 amino acid residues derived from frameshift (Fig. 1A). The VAP-C-specific antibody generated by immunization with the peptide corresponding to the residues from 86 to 98 clearly detected VAP-C but neither VAP-A nor VAP-B in cells transfected with expression plasmids encoding FLAG-tagged VAP-A, VAP-B, or VAP-C (Fig. 6A). To determine the distribution of VAPs in human organs, the pool lysates of various organs prepared from several people were examined by immunoblotting (Fig. 6B). Expression of VAP-A was detected clearly in the kidney, lung, prostate, and liver; slightly in the duodenum, uterus, vagina, and bladder; and barely in the small intestine and stomach. VAP-B was detected clearly in the bladder, kidney, and prostate and slightly in the duodenum, small intestine, uterus, vagina, and liver. Expression of VAP-C was detected clearly in the stomach, uterus, kidney, and bladder; slightly in the duodenum, small intestine, and prostate; and barely detected in the vagina, lung, and liver. Several bands smaller than the expected size of VAP-C were observed in the stomach, duodenum, small intestine, uterus, vagina, prostate, and bladder. Because the main target of HCV replication is thought to be the liver, we next examined the expression of VAPs in individual human liver samples. VAP-A and VAP-B were clearly detected in the liver tissues obtained from chronic hepatitis C patients and a healthy donor, but no expression of VAP-C was detected (Fig. 6C). These results suggest that the expression of VAP-C may participate in the determination of tissue tropism of HCV propagation.

Substitution of Ser for Pro^{56} in VAPs leads to suppression of HCV replication. A single mutation of Pro^{56} to Ser (P56S) of VAP-B has been reported to be highly associated with amyotrophic lateral sclerosis (ALS), and the P56S mutation of VAP-B but not of VAP-A has been shown to induce large

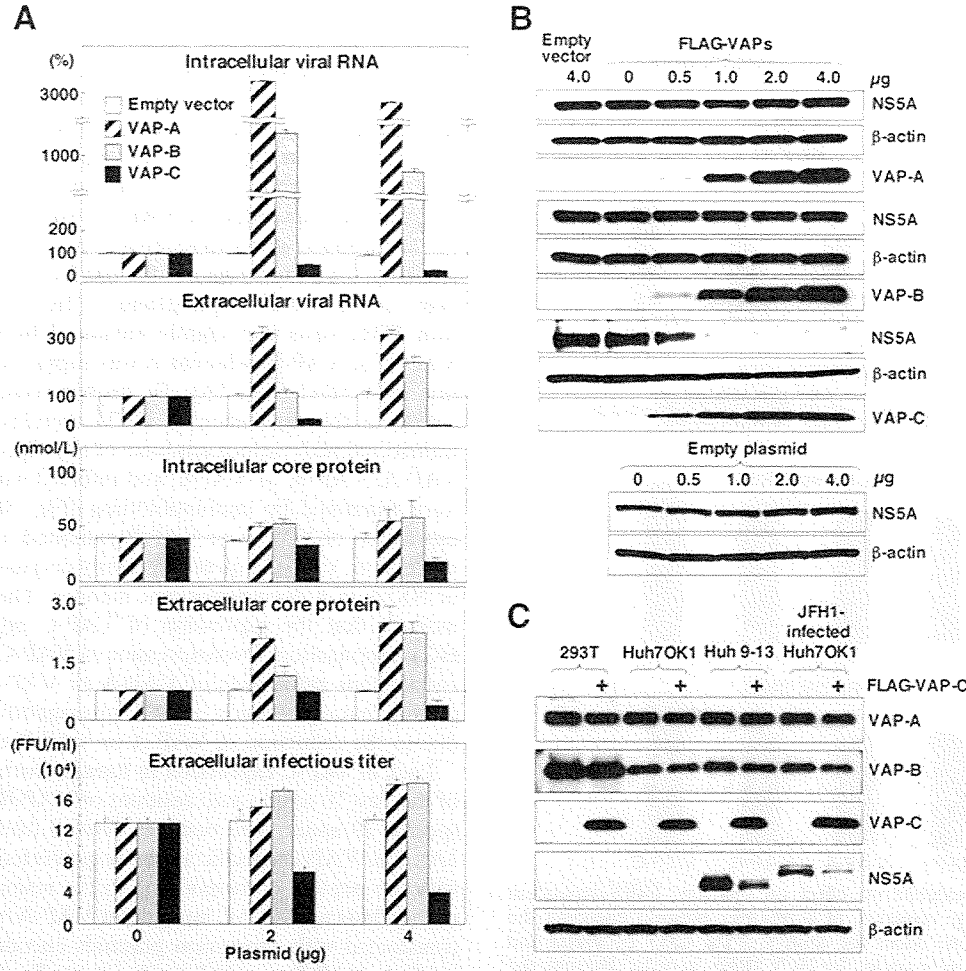

FIG. 5. VAP-C impairs HCV propagation but does not affect endogenous expression of VAP-A or VAP-B. Huh7OK1 cells transfected with 0 to 4 μg of plasmid encoding the FLAG-tagged VAP-A, VAP-B, or VAP-C or empty vector were infected with strain JFH1 at an MOI of 0.05 at 14 h posttransfection and then harvested at 96 h postinfection. (A) The intracellular and extracellular expression levels of viral RNA (top) and core protein (middle) were determined by real-time PCR and ELISA, respectively. Infectious viral titers in the culture supernatants were determined by focus-forming assay (bottom). Data in this panel are shown as the means ± standard deviations. (B) The expression levels of NS5A, β-actin, VAP-A, VAP-B, and VAP-C were determined by immunoblotting using anti-NS5A, anti-β-actin, or anti-FLAG tag antibody. (C) The embryonic kidney cell line (293T), the cured hepatoma cell line (Huh7OK1), and the replicon cell line (Huh 9-13) were transfected with 2 μg of the plasmid encoding FLAG-tagged VAP-C (+) or empty plasmid. In the case of the infected cells, Huh7OK1 cells were infected with strain JFH1 at an MOI of 0.05, reseeded onto the tissue culture plate at 96 h postinfection, and then transfected with 2 μg of the plasmids. These cells were harvested at 36 h posttransfection and examined by immunoblotting using antibodies to VAP-A, VAP-B, FLAG, NS5A, and β-actin. The data in each panel are representative of the results of three independent experiments.

aggregations of ER in culture cells and to sequester the wild-type protein into ubiquitinated inclusions (29, 37). To examine the effects on the replication of HCV of the P56S mutation in VAPs, FLAG-tagged VAP mutants were expressed in the HCV replicon cells. RNA replication of the subgenomic replicon in Huh 9-13 cells was impaired by the expression of each of the mutant VAPs (Fig. 7A, left). The expression of NS5A in the replicon cells was decreased by the expression of the mutant VAPs in a dose-dependent manner (Fig. 7A, right). Next, to examine the effect of the expression of the P56S VAP mutants on HCV propagation, Huh7OK1 cells expressing the FLAG-tagged VAP mutants were infected with JFH1 virus. The production of intracellular and extracellular viral RNA at 96 h postinfection was decreased by the expression of the P56S mutation in VAPs (Fig. 7B). Although the results of a previous study indicated that the expression of the P56S mutant of VAP-B but not that of VAP-A induced a large aggregation of ER in hamster ovary cell line CHO (37), the P56S mutants of VAP-A and VAP-B but not that of VAP-C exhibited accumulation of membranous aggregates in Huh 9-13 cells (Fig. 7C). These results indicate that the P56S mutation in both VAP-B and VAP-A induces aggregation of ER in human hepatoma cells, which in turn leads to the suppression of HCV propagation.

DISCUSSION

The replication of HCV has been shown to require several host proteins, including VAP-A/VAP-B (6, 9, 44), FBL2 (46), FKBP8 (34), hB-ind1 (40), Hsp90 (28, 34, 45), and cyclophilins

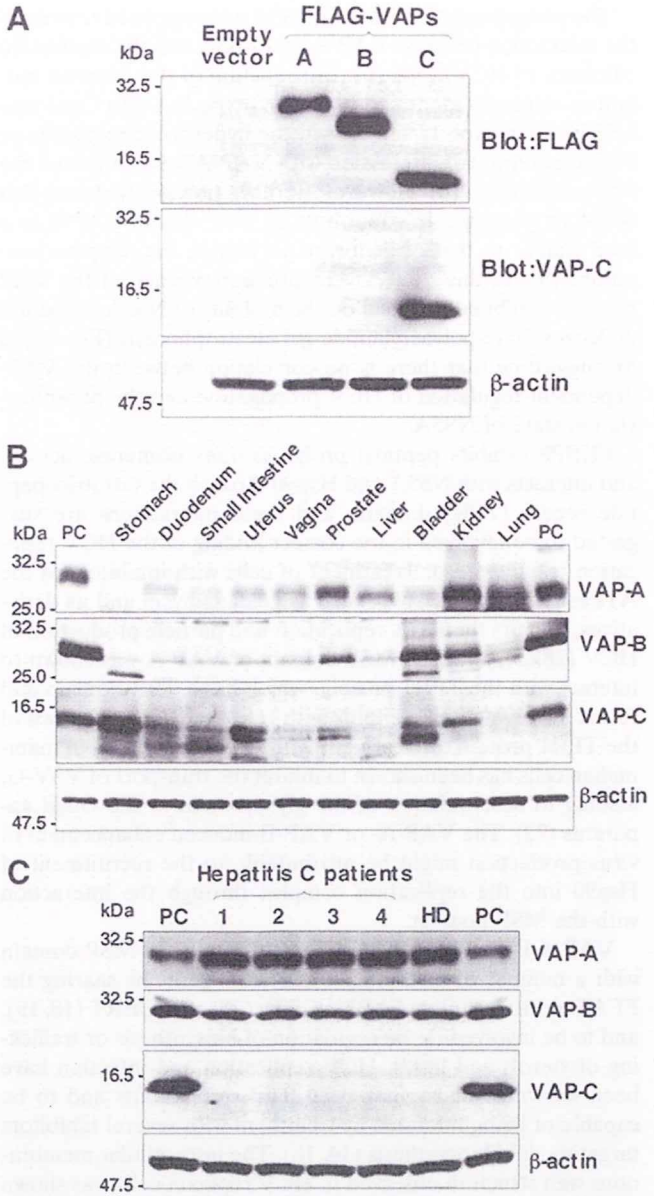

FIG. 6. Distribution of VAPs in human tissues. (A) Anti-VAP-C antibody specifically recognizes VAP-C. Human embryonic kidney 293T cells transfected with expression plasmid encoding FLAG-tagged VAP-A, VAP-B, or VAP-C or empty vector were harvested at 48 h posttransfection and examined by immunoblotting using anti-FLAG tag, anti-VAP-C, and anti-β-actin antibodies. (B) The premade human tissue lysates "Protein medleys" (20 μg each; Clonetech) were examined by immunoblotting using antibodies against VAP-A, VAP-B, VAP-C, or β-actin. (C) Expression of VAP family proteins in human liver tissues. Liver samples obtained from four hepatitis C patients (1 to 4) and one healthy donor (HD) were examined by immunoblotting as described above. The data in each panel are representative of the results of three independent experiments. PC indicates 293T cells transfected with expression plasmid encoding VAP-A, VAP-B, and VAP-C.

(15, 48). VAP-A has been detected in a detergent-resistant membrane fraction that was shown to be capable of replicating HCV RNA in vitro, and the interaction of VAP-A with NS5A is required for the efficient replication of HCV genomic RNA

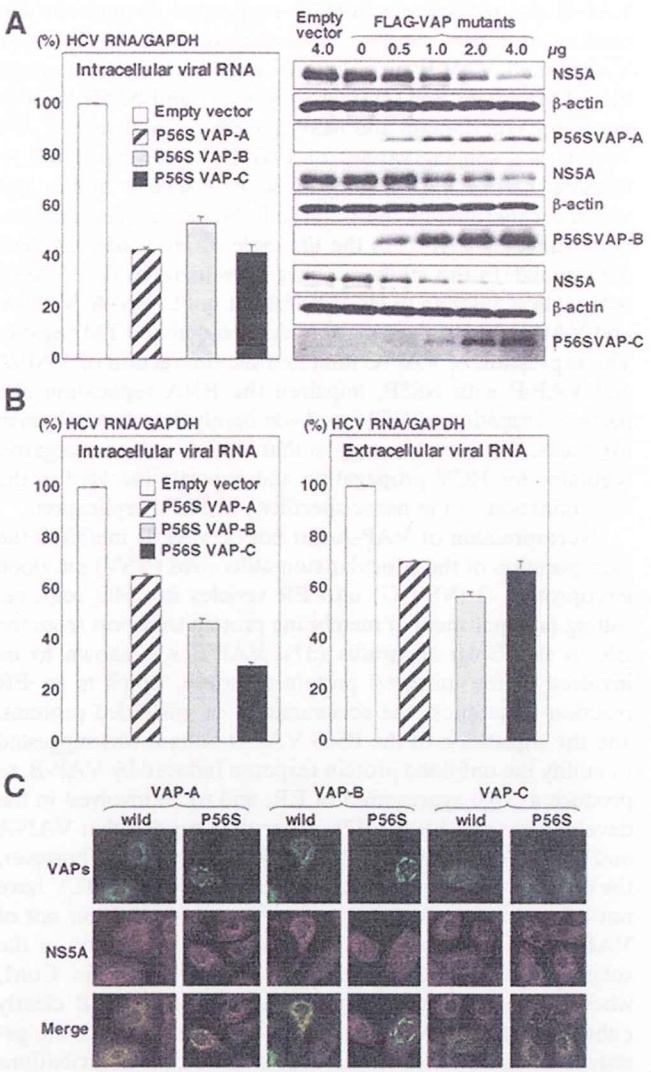

FIG. 7. Substitution of Ser for Pro^{56} in VAPs leads to suppression of HCV replication. (A) Left: Huh 9-13 cells were transfected with 4 μg of the expression plasmids encoding FLAG-tagged P56S VAP mutants or empty vector, and the level of intracellular HCV RNA was determined at 72 h posttransfection by real-time PCR after normalization with GAPDH mRNA. The value for HCV RNA at 0 h posttransfection in the cell line transfected with the empty plasmid is represented as 100%. Data in this panel are shown as the means ± standard deviations. Right: Huh 9-13 cells were transfected with 0 to 4 μg of the FLAG-tagged P56S VAP mutant plasmids or empty vector, and the levels of expression of NS5A, β-actin, and the mutant VAPs were determined by immunoblotting at 72 h posttransfection. The data in each panel are representative of the results of three independent experiments. (B) Huh7OK1 cells transfected with 4 μg of the expression plasmids encoding FLAG-tagged P56S VAP mutants or empty vector were infected with strain JFH1 at an MOI of 0.05 at 14 h posttransfection, and the intracellular (left) and extracellular (right) expression levels of viral RNA were determined by real-time PCR after normalization with GAPDH mRNA at 96 h postinfection. Data in this panel are shown as the means ± standard deviations. (C) Levels of expression of wild-type VAPs, P56S mutant VAPs, and NS5A in Huh 9-13 cells at 72 h after transfection with the expression plasmids encoding FLAG-tagged VAPs or P56S VAP mutants were determined by immunofluorescent assay. The data in each panel are representative of the results of three independent experiments.

(2, 7) and is modulated by the phosphorylation of NS5A (4, 6). VAP-B also participates in HCV replication through the formation of homo- and/or heterodimers with VAP-A (9). VAP-A and VAP-B form hetero- and homodimers through their TM regions and interact with NS5A and NS5B through the coiled-coil domain and MSP domain, respectively (9, 44). VAP-C is a splicing variant of VAP-B, consisting of the N-terminal half of VAP-B and the subtype-specific amino acid residues generated by the frameshift. However, the biological significance of VAP-C in the life cycle of HCV has not been determined. In this study, we have demonstrated that VAP-C is capable of binding to HCV NS5B but not to NS5A, VAP-A, and VAP-B due to the lack of the coiled-coil and TM regions. The expression of VAP-C inhibited the interaction of VAP-A and VAP-B with NS5B, impaired the RNA replication and particle formation of HCV, and was barely detected in human liver cells. These results suggest that VAP-C acts as a negative regulator for HCV propagation and is partly involved in the determination of the tissue specificity of HCV replication.

Overexpression of VAP-A but not of VAP-B inhibited the incorporation of the vesicular stomatitis virus (VSV) envelope glycoprotein G (VSV-G) into ER vesicles in CHO cells, resulting in impairment of membrane protein transport from the ER to the Golgi apparatus (37). VAP-B was shown to be involved in the unfolded protein response, which is an ER reaction to suppress the accumulation of misfolded proteins, and the expression of the P56S VAP-B mutant was suggested to nullify the unfolded protein response induced by VAP-B, to produce a large aggregation of ER, and to be involved in the development of ALS (17, 37). These data suggest that VAP-A and VAP-B possess different physiological functions; however, the contributions of the proteins to the life cycle of HCV have not been characterized. The expression of VAP-B but not of VAP-A resulted in an enhancement of the replication of the subgenomic HCV RNA of the genotype 1b strain Con1, whereas the expression of either VAP-A or VAP-B clearly enhanced viral RNA replication in cells infected with the genotype 2a strain JFH1 virus, suggesting that the contributions of VAP-A and VAP-B to viral RNA replication might differ among the genotypes of HCV. The expression of VAP-B or VAP-A enhanced RNA replication in the HCV replicon cells and the secretion of viral RNA, core protein, and infectious particles into the culture supernatants of Huh7OK1 cells infected with JFH1 virus, whereas the expression of these proteins had no effect on the expression of NS5A or on IRES-dependent translation. Thus, further studies will be needed to clarify the molecular mechanisms underlying the posttranslational enhancement of HCV production by the expression of VAP-A and VAP-B. In contrast to the expression of VAP-A and VAP-B, the expression of VAP-C clearly suppressed the RNA replication of both the genotype 1b RNA replicon cells and the genotype 2a strain JFH1 virus, by which both the expression of the viral proteins and the viral particle production were drastically impaired. Furthermore, the expression of the P56S mutants of VAP-A and VAP-B reduced RNA replication in HCV replicon cells and propagation of the JFH1 virus, probably due to the induction of aggregation of the ER. The reason why ER aggregation was induced by the expression of the P56S VAP-A mutant in Huh7 cells but not in CHO cells (17, 37) is not known at the moment.

The phosphorylation state of NS5A was suggested to control the interaction between VAP-A and NS5A and the replication efficiency of HCV RNA (6). Introduction of the adaptive mutations originally identified in the genotype 1b strain Con1 into NS5A of genotype 1a suppressed the hyperphosphorylation of NS5A, potentiated interaction with VAP-A, and enhanced the RNA replication (6). However, we have previously shown that NS5A of genotype 1a could bind to VAP-A and VAP-B at a level similar to that of genotype 1b despite the adaptive mutations (9). In this study, overexpression of each of the VAP proteins exhibited no effect on the mobility of NS5A in sodium dodecyl sulfate-polyacrylamide gel electrophoresis (Fig. 3 and 5), suggesting that there is no correlation between the VAP-dependent regulation of HCV propagation and the phosphorylation state of NS5A.

FKBP8 exhibits peptidyl prolyl *cis-trans* isomerase activity and interacts with NS5A and Hsp90 through the tetratricopeptide repeat (TPR) domain, and these interactions are suggested to be involved in the correct folding of the HCV replication complex (34). Treatment of cells with inhibitors of the ATPase activity of Hsp90, such as geldanamycin and its derivatives, impairs the RNA replication and particle production of HCV (28, 34, 45). The MSP domain of VAP-A was shown to interact with the TPR1 protein, which has a TPR domain and forms the chaperone complex with Hsp90 (22). Knockdown of the TPR1 protein or treatment with Hsp90 inhibitors in mammalian cells has been shown to inhibit the transport of VSV-G, leading to accumulation of the glycoprotein in the Golgi apparatus (22). The VAP-A- or VAP-B-induced enhancement of virus production might be attributable to the recruitment of Hsp90 into the replication complex through the interaction with the MSP domain.

VAP-A is well known to interact through the MSP domain with a number of mammalian and yeast proteins sharing the FFAT motif, including OSBPs, ORPs (20), and CERT (10, 19), and to be involved in the regulation of biosynthesis or trafficking of sterols and lipids. HCV replication and infection have been shown to be regulated by lipid components and to be capable of being inhibited by treatment with several inhibitors targeting lipid biosynthesis (14, 18). The intracellular membranous web structure observed in HCV replicon cells was shown to be resistant to detergent treatment, suggesting that the lipid raft-like structure abundant in cholesterol and sphingolipid is generated by the replication of HCV RNA (2, 24). Therefore, it might be feasible to speculate that VAP-A and VAP-B are involved in the construction of the HCV replication complex consisting of viral proteins and host cellular lipid components and that VAP-C interrupts the VAP-A and VAP-B functions and negatively regulates HCV propagation. Although the molecular mechanisms and the biological significance remain to be clarified, the MSP domain of VAP proteins was processed in human leukocytes and secreted into human serum (43). Further studies are needed to clarify the biogenesis and biological functions of the truncated VAP proteins in the replication of HCV.

In summary, we have shown that VAP-C is capable of suppressing the RNA replication and particle production of HCV by inhibiting the binding of VAP-A and VAP-B to NS5B through the N-terminal half of its MSP domain. The clear suppression of HCV propagation by the expression of VAP-C

further suggests the possibility of developing a novel therapeutic measure to eliminate HCV by the exogenous expression of VAP-C in the hepatocytes of chronic hepatitis C patients.

ACKNOWLEDGMENTS

We thank H. Murase for her secretarial work. We also thank R. Bartenschlager and T. Wakita for providing cell lines and plasmids.

This work was supported in part by grants-in-aid from the Ministry of Health, Labor, and Welfare; the Ministry of Education, Culture, Sports, Science, and Technology; the Global Center of Excellence Program; and the Foundation for Biomedical Research and Innovation.

REFERENCES

1. **Abe, T., Y. Kaname, I. Hamamoto, Y. Tsuda, X. Wen, S. Taguwa, K. Moriishi, O. Takeuchi, T. Kawai, T. Kanto, N. Hayashi, S. Akira, and Y. Matsuura.** 2007. Hepatitis C Virus nonstructural protein 5A modulates Toll-like receptor-MyD88-dependent signaling pathway in the macrophage cell lines. J. Virol. **81**:8953–8966.
2. **Aizaki, H., K. J. Lee, V. M. Sung, H. Ishiko, and M. M. Lai.** 2004. Characterization of the hepatitis C virus RNA replication complex associated with lipid rafts. Virology **324**:450–461.
3. **Behrens, S. E., L. Tomei, and R. De Francesco.** 1996. Identification and properties of the RNA-dependent RNA polymerase of hepatitis C virus. EMBO J. **15**:12–22.
4. **Blight, K. J., A. A. Kolykhalov, and C. M. Rice.** 2000. Efficient initiation of HCV RNA replication in cell culture. Science **290**:1972–1974.
5. **Egger, D., B. Wolk, R. Gosert, L. Bianchi, H. E. Blum, D. Moradpour, and K. Bienz.** 2002. Expression of hepatitis C virus proteins induces distinct membrane alterations including a candidate viral replication complex. J. Virol. **76**:5974–5984.
6. **Evans, M. J., C. M. Rice, and S. P. Goff.** 2004. Phosphorylation of hepatitis C virus nonstructural protein 5A modulates its protein interactions and viral RNA replication. Proc. Natl. Acad. Sci. USA **101**:13038–13043.
7. **Gao, L., H. Aizaki, J.-W. He, and M. M. C. Lai.** 2004. Interactions between viral nonstructural proteins and host protein hVAP-33 mediate the formation of hepatitis C virus RNA replication complex on lipid raft. J. Virol. **78**:3480–3488.
8. **Grakoui, A., D. W. McCourt, C. Wychowski, S. M. Feinstone, and C. M. Rice.** 1993. Characterization of the hepatitis C virus-encoded serine proteinase: determination of proteinase-dependent polyprotein cleavage sites. J. Virol. **67**:2832–2843.
9. **Hamamoto, I., Y. Nishimura, T. Okamoto, H. Aizaki, M. Liu, Y. Mori, T. Abe, T. Suzuki, M. M. Lai, T. Miyamura, K. Moriishi, and Y. Matsuura.** 2005. Human VAP-B is involved in hepatitis C virus replication through interaction with NS5A and NS5B. J. Virol. **79**:13473–13482.
10. **Hanada, K., K. Kumagai, S. Yasuda, Y. Miura, M. Kawano, M. Fukasawa, and M. Nishijima.** 2003. Molecular machinery for non-vesicular trafficking of ceramide. Nature **426**:803–809.
11. **Ho, S. N., H. D. Hunt, R. M. Horton, J. K. Pullen, and L. R. Pease.** 1989. Site-directed mutagenesis by overlap extension using the polymerase chain reaction. Gene **77**:51–59.
12. **Hoofnagle, J. H.** 2002. Course and outcome of hepatitis C. Hepatology **36**:S21–S29.
13. **Huang, D. C., S. Cory, and A. Strasser.** 1997. Bcl-2, Bcl-XL and adenovirus protein E1B19kD are functionally equivalent in their ability to inhibit cell death. Oncogene **14**:405–414.
14. **Ikeda, M., K. Abe, M. Yamada, H. Dansako, K. Naka, and N. Kato.** 2006. Different anti-HCV profiles of statins and their potential for combination therapy with interferon. Hepatology **44**:117–125.
15. **Inoue, K., T. Umehara, U. T. Ruegg, F. Yasui, T. Watanabe, H. Yasuda, J. M. Dumont, P. Scalfaro, M. Yoshiba, and M. Kohara.** 2007. Evaluation of a cyclophilin inhibitor in hepatitis C virus-infected chimeric mice in vivo. Hepatology **45**:921–928.
16. **Kaiser, S. E., J. H. Brickner, A. R. Reilein, T. D. Fenn, P. Walter, and A. T. Brunger.** 2005. Structural basis of FFAT motif-mediated ER targeting. Structure **13**:1035–1045.
17. **Kanekura, K., I. Nishimoto, S. Aiso, and M. Matsuoka.** 2006. Characterization of amyotrophic lateral sclerosis-linked P56S mutation of vesicle-associated membrane protein-associated protein B (VAPB/ALS8). J. Biol. Chem. **281**:30223–30233.
18. **Kapadia, S. B., and F. V. Chisari.** 2005. Hepatitis C virus RNA replication is regulated by host geranylgeranylation and fatty acids. Proc. Natl. Acad. Sci. USA **102**:2561–2566.
19. **Kawano, M., K. Kumagai, M. Nishijima, and K. Hanada.** 2006. Efficient trafficking of ceramide from the endoplasmic reticulum to the Golgi apparatus requires a VAMP-associated protein-interacting FFAT motif of CERT. J. Biol. Chem. **281**:30279–30288.
20. **Loewen, C. J., A. Roy, and T. P. Levine.** 2003. A conserved ER targeting motif in three families of lipid binding proteins and in Opi1p binds VAP. EMBO J. **22**:2025–2035.
21. **Lohmann, V., F. Korner, J. Koch, U. Herian, L. Theilmann, and R. Bartenschlager.** 1999. Replication of subgenomic hepatitis C virus RNAs in a hepatoma cell line. Science **285**:110–113.
22. **Lotz, G. P., A. Brychzy, S. Heinz, and W. M. Obermann.** 2008. A novel HSP90 chaperone complex regulates intracellular vesicle transport. J. Cell Sci. **121**:717–723.
23. **McLauchlan, J., M. K. Lemberg, G. Hope, and B. Martoglio.** 2002. Intramembrane proteolysis promotes trafficking of hepatitis C virus core protein to lipid droplets. EMBO J. **21**:3980–3988.
24. **Miyanari, Y., M. Hijikata, M. Yamaji, M. Hosaka, H. Takahashi, and K. Shimotohno.** 2003. Hepatitis C virus non-structural proteins in the probable membranous compartment function in viral genome replication. J. Biol. Chem. **278**:50301–50308.
25. **Moriishi, K., and Y. Matsuura.** 2007. Host factors involved in the replication of hepatitis C virus. Rev. Med. Virol. **17**:343–354.
26. **Moriishi, K., and Y. Matsuura.** 2003. Mechanisms of hepatitis C virus infection. Antivir. Chem. Chemother. **14**:285–297.
27. **Moriishi, K., T. Okabayashi, K. Nakai, K. Moriya, K. Koike, S. Murata, T. Chiba, K. Tanaka, R. Suzuki, T. Suzuki, T. Miyamura, and Y. Matsuura.** 2003. Proteasome activator PA28gamma-dependent nuclear retention and degradation of hepatitis C virus core protein. J. Virol. **77**:10237–10249.
28. **Nakagawa, S., T. Umehara, C. Matsuda, S. Kuge, M. Sudoh, and M. Kohara.** 2007. Hsp90 inhibitors suppress HCV replication in replicon cells and humanized liver mice. Biochem. Biophys. Res. Commun. **353**:882–888.
29. **Nishimura, A. L., M. Mitne-Neto, H. C. Silva, A. Richieri-Costa, S. Middleton, D. Cascio, F. Kok, J. R. Oliveira, T. Gillingwater, J. Webb, P. Skehel, and M. Zatz.** 2004. A mutation in the vesicle-trafficking protein VAPB causes late-onset spinal muscular atrophy and amyotrophic lateral sclerosis. Am. J. Hum. Genet. **75**:822–831.
30. **Nishimura, Y., M. Hayashi, H. Inada, and T. Tanaka.** 1999. Molecular cloning and characterization of mammalian homologues of vesicle-associated membrane protein-associated (VAMP-associated) proteins. Biochem. Biophys. Res. Commun. **254**:21–26.
31. **Niwa, H., K. Yamamura, and J. Miyazaki.** 1991. Efficient selection for high-expression transfectants with a novel eukaryotic vector. Gene **108**:193–199.
32. **Okamoto, K., Y. Mori, Y. Komoda, T. Okamoto, M. Okochi, M. Takeda, T. Suzuki, K. Moriishi, and Y. Matsuura.** 2008. Intramembrane processing by signal peptide peptidase regulates the membrane localization of hepatitis C virus core protein and viral propagation. J. Virol. **82**:8349–8361.
33. **Okamoto, K., K. Moriishi, T. Miyamura, and Y. Matsuura.** 2004. Intramembrane proteolysis and endoplasmic reticulum retention of hepatitis C virus core protein. J. Virol. **78**:6370–6380.
34. **Okamoto, T., Y. Nishimura, T. Ichimura, K. Suzuki, T. Miyamura, T. Suzuki, K. Moriishi, and Y. Matsuura.** 2006. Hepatitis C virus RNA replication is regulated by FKBP8 and Hsp90. EMBO J. **25**:5015–5025.
35. **Okamoto, T., H. Omori, Y. Kaname, T. Abe, Y. Nishimura, T. Suzuki, T. Miyamura, T. Yoshimori, K. Moriishi, and Y. Matsuura.** 2008. A single-amino-acid mutation in hepatitis C virus NS5A disrupting FKBP8 interaction impairs viral replication. J. Virol. **82**:3480–3489.
36. **Pennetta, G., P. R. Hiesinger, R. Fabian-Fine, I. A. Meinertzhagen, and H. J. Bellen.** 2002. Drosophila VAP-33A directs bouton formation at neuromuscular junctions in a dosage-dependent manner. Neuron **35**:291–306.
37. **Prosser, D. C., D. Tran, P. Y. Gougeon, C. Verly, and J. K. Ngsee.** 2008. FFAT rescues VAPA-mediated inhibition of ER-to-Golgi transport and VAPB-mediated ER aggregation. J. Cell Sci. **121**:3052–3061.
38. **Skehel, P. A., R. Fabian-Fine, and E. R. Kandel.** 2000. Mouse VAP33 is associated with the endoplasmic reticulum and microtubules. Proc. Natl. Acad. Sci. USA **97**:1101–1106.
39. **Skehel, P. A., K. C. Martin, E. R. Kandel, and D. Bartsch.** 1995. A VAMP-binding protein from *Aplysia* required for neurotransmitter release. Science **269**:1580–1583.
40. **Taguwa, S., T. Okamoto, T. Abe, Y. Mori, T. Suzuki, K. Moriishi, and Y. Matsuura.** 2008. Human butyrate-induced transcript 1 interacts with hepatitis C virus NS5A and regulates viral replication. J. Virol. **82**:2631–2641.
41. **Tellinghuisen, T. L., J. Marcotrigiano, and C. M. Rice.** 2005. Structure of the zinc-binding domain of an essential component of the hepatitis C virus replicase. Nature **435**:374–379.
42. **Tomei, L., C. Failla, E. Santolini, R. De Francesco, and N. La Monica.** 1993. NS3 is a serine protease required for processing of hepatitis C virus polyprotein. J. Virol. **67**:4017–4026.
43. **Tsuda, H., S. M. Han, Y. Yang, C. Tong, Y. Q. Lin, K. Mohan, C. Haueter, A. Zoghbi, Y. Harati, J. Kwan, M. A. Miller, and H. J. Bellen.** 2008. The amyotrophic lateral sclerosis 8 protein VAPB is cleaved, secreted, and acts as a ligand for Eph receptors. Cell **133**:963–977.
44. **Tu, H., L. Gao, S. T. Shi, D. R. Taylor, T. Yang, A. K. Mircheff, Y. Wen, A. E. Gorbalenya, S. B. Hwang, and M. M. Lai.** 1999. Hepatitis C virus RNA polymerase and NS5A complex with a SNARE-like protein. Virology **263**: 30–41.

45. **Ujino, S., S. Yamaguchi, K. Shimotohno, and H. Takaku.** 2009. Heat-shock protein 90 is essential for stabilization of the hepatitis C virus non-structural protein NS3. J. Biol. Chem. **284**:6841–6846.
46. **Wang, C., M. Gale, Jr., B. C. Keller, H. Huang, M. S. Brown, J. L. Goldstein, and J. Ye.** 2005. Identification of FBL2 as a geranylgeranylated cellular protein required for hepatitis C virus RNA replication. Mol. Cell **18**:425–434.
47. **Wasley, A., and M. J. Alter.** 2000. Epidemiology of hepatitis C: geographic differences and temporal trends. Semin. Liver Dis. **20**:1–16.
48. **Watashi, K., N. Ishii, M. Hijikata, D. Inoue, T. Murata, Y. Miyanari, and K. Shimotohno.** 2005. Cyclophilin B is a functional regulator of hepatitis C virus RNA polymerase. Mol. Cell **19**:111–122.
49. **Weir, M. L., A. Klip, and W. S. Trimble.** 1998. Identification of a human homologue of the vesicle-associated membrane protein (VAMP)-associated protein of 33 kDa (VAP-33): a broadly expressed protein that binds to VAMP. Biochem. J. **333**:247–251.
50. **Weir, M. L., H. Xie, A. Klip, and W. S. Trimble.** 2001. VAP-A binds promiscuously to both v- and tSNAREs. Biochem. Biophys. Res. Commun. **286**:616–621.
51. **Zhong, J., P. Gastaminza, G. Cheng, S. Kapadia, T. Kato, D. R. Burton, S. F. Wieland, S. L. Uprichard, T. Wakita, and F. V. Chisari.** 2005. Robust hepatitis C virus infection in vitro. Proc. Natl. Acad. Sci. USA **102**:9294–9299.

JOURNAL OF VIROLOGY, Aug. 2009, p. 7629–7640 Vol. 83, No. 15
0022-538X/09/$08.00+0 doi:10.1128/JVI.00679-09

Baculovirus Induces Type I Interferon Production through Toll-Like Receptor-Dependent and -Independent Pathways in a Cell-Type-Specific Manner▽

Takayuki Abe,[1] Yuuki Kaname,[1] Xiaoyu Wen,[1] Hideki Tani,[1] Kohji Moriishi,[1] Satoshi Uematsu,[2] Osamu Takeuchi,[2] Ken J. Ishii,[2] Taro Kawai,[2] Shizuo Akira,[2] and Yoshiharu Matsuura[1]*

Department of Molecular Virology, Research Institute for Microbial Diseases,[1] and Laboratory of Host Defense, WPI Immunology Frontier Research Center,[2] Osaka University, Osaka, Japan

Received 2 April 2009/Accepted 19 May 2009

***Autographa californica* nuclear polyhedrosis virus (AcNPV) is a double-stranded-DNA virus that is pathogenic to insects. AcNPV was shown to induce an innate immune response in mammalian immune cells and to confer protection of mice from lethal viral infection. In this study, we have shown that production of type I interferon (IFN) by AcNPV in murine plasmacytoid dendritic cells (pDCs) and non-pDCs, such as peritoneal macrophages and splenic CD11c$^+$ DCs, was mediated by Toll-like receptor (TLR)-dependent and -independent pathways, respectively. IFN regulatory factor 7 (IRF7) was shown to play a crucial role in the production of type I IFN by AcNPV not only in immune cells in vitro but also in vivo. In mouse embryonic fibroblasts (MEFs), AcNPV produced IFN-β and IFN-inducible chemokines through TLR-independent and IRF3-dependent pathways, in contrast to the TLR-dependent and IRF3/IRF7-independent production of proinflammatory cytokines. Although production of IFN-β and IFN-inducible chemokines was severely impaired in IFN promoter-stimulator 1 (IPS-1)-deficient MEFs upon infection with vesicular stomatitis virus, AcNPV produced substantial amounts of the cytokines in IPS-1-deficient MEFs. These results suggest that a novel signaling pathway(s) other than TLR- and IPS-1-dependent pathways participates in the production of type I IFN in response to AcNPV infection.**

The baculovirus *Autographa californica* nuclear polyhedrosis virus (AcNPV) is an enveloped, double-stranded-DNA (dsDNA) virus that is pathogenic primarily to insects. AcNPV has long been used as an efficient gene expression vector in insect cells (31, 35). Recently, baculovirus was shown to be capable of infecting various mammalian cells without any replication and of expressing foreign genes under the control of a mammalian promoter (28). Therefore, baculovirus is now recognized as a useful viral vector not only for abundant gene expression in insect cells but also for gene delivery into mammalian cells.

In addition to allowing efficient gene delivery, AcNPV has been shown to stimulate interferon (IFN) production in mammalian cell lines and confer protection from lethal virus infection in mice (2, 12). Furthermore, AcNPV was shown to possess a strong adjuvant activity to promote humoral and cellular immune responses against coadministered antigens, maturation of dendritic cells (DCs), and production of proinflammatory cytokines, chemokines, and type I IFNs (14). However, the precise mechanisms by which AcNPV induces a strong innate immune response in mice remain unclear. We have demonstrated previously that AcNPV activates the production of proinflammatory cytokines in peritoneal macrophages (PECs), splenic CD11c$^+$ DCs, and the murine macrophage line RAW264.7 through a Toll-like receptor 9 (TLR9)/MyD88-dependent pathway (1). However, significant amounts of IFN-α were still detectable in the PECs and splenic CD11c$^+$ DCs derived from TLR9- or MyD88-deficient mice in response to AcNPV, suggesting that TLR9/MyD88-independent pathways are involved in the production of type I IFN by AcNPV in the PECs and splenic CD11c$^+$ DCs (1).

Induction of type I IFN by pathogens is crucial for innate immunity, and such induction is mediated by the activation of pattern recognition receptors, such as TLRs and cytosolic receptors, including retinoic acid-inducible protein I (RIG-I) and melanoma differentiation-associated gene 5 (MDA5) (24, 49, 50). Type I IFN induction is controlled primarily at the gene transcriptional level, wherein a family of transcription factors, IFN regulatory factors (IRFs), plays a pivotal role (16). IRF3 and IRF7 are now known to be essential for the RIG-I-, MDA5-, and TLR-mediated type I IFN production pathway. IRF3 is induced by a primary response to initiate IFN-β production, whereas IRF7 is induced by IFN-β and participates in the late phase of IFN-α induction (16). All TLRs, except for TLR3, activate the MyD88-dependent pathway, whereas TLR3 and TLR4 activate the TRIF-dependent pathway. There is accumulating evidence that IRFs are activated by the MyD88- and TRIF-dependent signaling pathways and contribute to the activation of the type I IFN gene (24). RIG-I and MDA5 contain a C-terminal DExD/H-box RNA helicase domain required for the interaction with dsRNA and two N-terminal caspase recruitment and activation domains (CARDs) responsible for the activation of downstream IRF3, IRF7, and NF-κB signaling pathways (49).

Plasmacytoid DCs (pDCs) have been identified as the major cells involved in the production of type I IFN in response to viral stimulation (3, 6). The type I IFN production in the pDCs was dependent on the TLR signaling pathway, whereas that in non-pDC immune cells, including macrophages, conventional

* Corresponding author. Mailing address: Department of Molecular Virology, Research Institute for Microbial Diseases, Osaka University, 3-1 Yamada-oka, Suita, Osaka 565-0871, Japan. Phone: 81-6-6879-8340. Fax: 81-6-6879-8269. E-mail: matsuura@biken.osaka-u.ac.jp.

▽ Published ahead of print on 27 May 2009.

DCs, and mouse embryonic fibroblasts (MEFs), was dependent on the RIG-I/MDA5 signaling pathways (23). On the other hand, recent studies have also shown that non-pDC immune cells participate in the production of type I IFN in response to viral infection through TLR-dependent and TLR-independent pathways (9, 34). Viral genomic DNA of adenovirus (38, 53) and herpes simplex virus type 1 (HSV-1) (15) produces type I IFN through both TLR-dependent and -independent pathways. Modified vaccinia virus Ankara has also been shown to induce TLR-independent type I IFN production (46). Furthermore, nonprofessional immune cells, such as fibroblasts, were shown to produce type I IFN upon viral infection through a TLR-independent pathway (23). Infection with intracellular bacteria or introduction of synthetic dsDNA also induces production of type I IFN through a TLR- or an RNA helicase-independent pathway (19), suggesting the existence of a cytosolic DNA-sensing mechanism which stimulates the production of type I IFN (4, 5, 43). These results suggest that genomes of DNA viruses and intracellular bacteria produce type I IFN through a not-yet-identified cytosolic DNA-sensing machinery.

In this study, we have examined the mechanism of production of type I IFN in both pDCs and non-pDCs in response to AcNPV stimulation. The levels of involvement of the TLR or the RNA helicase pathway in the production of type I IFN in response to AcNPV stimulation differed among cell types, and the production was completely dependent on IRF7 in both pDCs and non-pDCs, such as PECs and splenic CD11c$^+$ DCs, whereas it was dependent on IRF3 in MEFs. These results suggest that AcNPV is capable of producing type I IFN through both TLR9-dependent and -independent pathways and might be an ideal tool for elucidating the mechanisms of the induction of type I IFN by DNA in mammalian cells.

MATERIALS AND METHODS

Mice and MEFs. C57BL/6 mice were purchased from CLEA Japan (Tokyo, Japan). MyD88-, TLR3-, TLR7-, TLR9-, IFN-αβ receptor (IFNR)-, RIG-I-, or IFN promoter-stimulator 1 (IPS-1)-deficient mice and MEFs from mice with a double knockout of MyD88 and TRIF, RIG-I, or IPS-1 were described previously (13, 23, 30, 48). IRF3- and IRF7-deficient mice (18) were purchased from Riken BioResource Center (Tsukuba, Japan), and the MEFs from the deficient mice were obtained from day 12.5 to 13.5 embryos. MEFs were maintained in Dulbecco's modified Eagle's medium (Sigma, St. Louis, MO) supplemented with 10% heat-inactivated fetal calf serum, 1.5 mM L-glutamine, 100 U/ml penicillin, and 100 μg/ml streptomycin at 37°C in a humidified atmosphere, with 5% CO_2.

Viruses and reagents. AcNPV was propagated in *Spodoptera frugiperda* (Sf-9) cells in Sf-900II insect medium (Invitrogen, Tokyo, Japan) supplemented with 10% heat-inactivated fetal calf serum. AcNPV and viral DNA were purified as previously described (1). Phosphorothioate-stabilized mouse CpG (mCpG) oligodeoxynucleotides (ODN1668) (TCC-ATG-ACG-TTC-CTG-ATG-CT) were purchased from Invitrogen. Endotoxin-free bacterial DNA from *Escherichia coli* K-12, poly(I:C), and imiquimod (R-837), an imidazoquinoline amine analogue to guanosine, were purchased from InvivoGen (San Diego, CA). Lipopolysaccharide (LPS) derived from *Salmonella enterica* serovar Minnesota (Re-595) and chloroquine were purchased from Sigma. Vesicular stomatitis virus (VSV) variants GLPLF and NCP12.1, derived from Indiana strains, were kindly provided by M. A. Whitt (22). The virus stocks and the other TLR ligands were free of endotoxin (<0.01 endotoxin units/ml), as determined using a Pyrodick endotoxin measurement kit (Seikagaku Co., Tokyo, Japan).

Production of truncated forms of gp64 protein. A recombinant baculovirus possessing a cDNA encoding a deletion mutant of gp64 lacking a transmembrane region (gp64ΔTM) was produced as described previously (1) by using a Bac-to-Bac baculovirus expression system according to the manufacturer's instructions (Invitrogen). At 3 days after infection with the recombinant virus, the recombinant gp64 protein was purified from the culture supernatants by use of a column of nickel-nitrilotriacetic acid beads (Qiagen, Valencia, CA). The protein concentrations were determined by using a Micro BCA protein assay kit (Pierce, Rockford, IL). The recombinant proteins were analyzed by sodium dodecyl sulfate-12.5% polyacrylamide gel electrophoresis under reducing conditions, stained with GelCord Blue stain reagent (Pierce), and detected by immunoblot analysis using antihexahistidine monoclonal antibody (Santa Cruz Biotechnology, Santa Cruz, CA) or anti-gp64 (AcV5), kindly provided by P. Faulkner.

Preparation of PECs and splenic DCs. To evaluate cytokine production in macrophages in vitro, mice were intraperitoneally injected with 2 ml of 4% thioglycolate (Sigma), and exudation cells were harvested at 3 days posttreatment by peritoneal lavage. Thioglycolate-elicited PECs were seeded into 96-well plates at a concentration of 2×10^5 cells/well and treated with various doses of stimuli. After 24 h of incubation, culture supernatants were harvested and analyzed for cytokine production. To prepare splenocytes containing DCs or pDCs, spleen tissue was cut into small fragments and incubated with RPMI 1640 medium containing 400 U/ml collagenase (Wako, Tokyo, Japan) and 15 μg/ml DNase (Sigma) at 37°C for 20 min. For the last 5 min, 5 mM EDTA was added, and single-cell suspensions were prepared after red blood cell lysis. Splenic CD11c$^+$ DCs and pDCs were purified by a magnetic cell sorter system with anti-CD11c and anti-murine plasmacytoid dendritic cell antigen 1 microbeads (Miltenyi Biotec GmbH, Bergisch Gladbach, Germany), respectively, following the manufacturer's instructions. Enriched cells containing >90% splenic CD11c$^+$ DCs and pDCs were seeded into 96-well plates at a concentration of 2×10^5 cells/well.

Production of cytokines in vitro and in vivo. Production of IFNs (IFN-α and -β) and proinflammatory cytokines (interleukin-6 [IL-6] and IL-12) in the culture supernatants was determined by use of enzyme-linked immunosorbent assay (ELISA) kits purchased from PBL Biomedical Laboratories (New Brunswick, NJ) and BD PharMingen (San Diego, CA), respectively. To determine the effects of endosomal maturation on cytokine production by infection with AcNPV or transfection of baculoviral DNA, PECs and splenic CD11c$^+$ DCs were seeded into 96-well plates at a concentration of 2×10^5 cells/well and inoculated with AcNPV or transfected with the viral DNA encapsulated in liposomes in the presence or absence of endosomal inhibitors, such as chloroquine. AcNPV (100 μg/mouse) was intraperitoneally inoculated into wild-type mice and mice with knockout of the MyD88, TLR9, IFNR, or IRF7 gene, and levels of production of IL-12, IL-6, and IFN-α in sera were determined at different time points.

Quantitative analyses of cytokine mRNA. MEFs derived from wild-type mice; mice with knockout of the IRF3, IRF7, RIG-I, or IPS-1 gene; and mice with double knockout of the MyD88 and TRIF genes were stimulated with AcNPV, VSV, LPS, gp64ΔTM, AcNPV DNA, or poly(I:C). At 4 to 8 h posttreatment, total RNA was prepared from the MEFs by using an RNeasy mini kit (Qiagen). First-strand cDNA was synthesized by using a ReverTra Ace kit (Toyobo, Osaka, Japan) and an oligo(dT)$_{20}$ primer. Each cDNA was estimated by use of Platinum SYBR green qPCR SuperMix UDG (Invitrogen) according to the manufacturer's protocol. Fluorescent signals were analyzed with an ABI Prism 7000 instrument (Applied Biosystems, Tokyo, Japan). The mouse IFN-α1, IFN-β, MCP-1 (monocyte chemoattractant protein 1), IP-10, RANTES, IL-6, and GAPDH (glyceraldehyde-3-phosphate dehydrogenase) genes were amplified using the primer pairs 5′-AGCCTTGACACTCCTGGTACAAATG-3′ and 5′-TGGGTC AGCTCACTCAGGACA-3′, 5′-ACACCAGCCTGGCTTCCATC-3′ and 5′-TT GGAGCTGGAGCTGCTTATAGTTG-3′, 5′-GCATCCACGTGTTGGCTC A-3′ and 5′-CTCCAGCCTACTCATTGGGATCA-3′, 5′-TGAATCCGGAATC TAAGACCATCAA-3′ and 5′-AGGACTAGCCATCCACTGGGTAAAG-3′, 5′-GCTCAAGCCATCCTTGTGCTAA-3′ and 5′-CATTGAGCTGATGGAG GTC-3′, 5′-TTGGTTAAATGACCTGCAACAGGA-3′ and 5′-CCACTTCACA AGTCGGAGGCTTA-3′, and 5′-ACCACAGTCCATGCCATCAC-3′ and 5′-T CCACCACCCTGTTGCTGTA-3′, respectively. The expression of the mRNAs of each of the cytokines was normalized to that of GAPDH mRNA.

In vitro cytopathic-effect assays. Induction of an antiviral state by AcNPV in vitro was determined by the cytopathic-effect assay, as described previously (12). Briefly, MEFs seeded in triplicate in 96-well tissue culture plates (2×10^3 cells/well) were incubated with serial dilutions of AcNPV, poly(I:C), or mCpG and washed with medium after 24 h of incubation. Then, VSV (GLPLF strain) was inoculated at a multiplicity of infection (MOI) of 0.1. Cell viability was determined by crystal violet staining at 24 h postinfection.

RESULTS

Involvement of TLR-dependent and -independent pathways in the production of type I IFN by AcNPV in immune cells and in mice. We have reported previously that AcNPV is capable

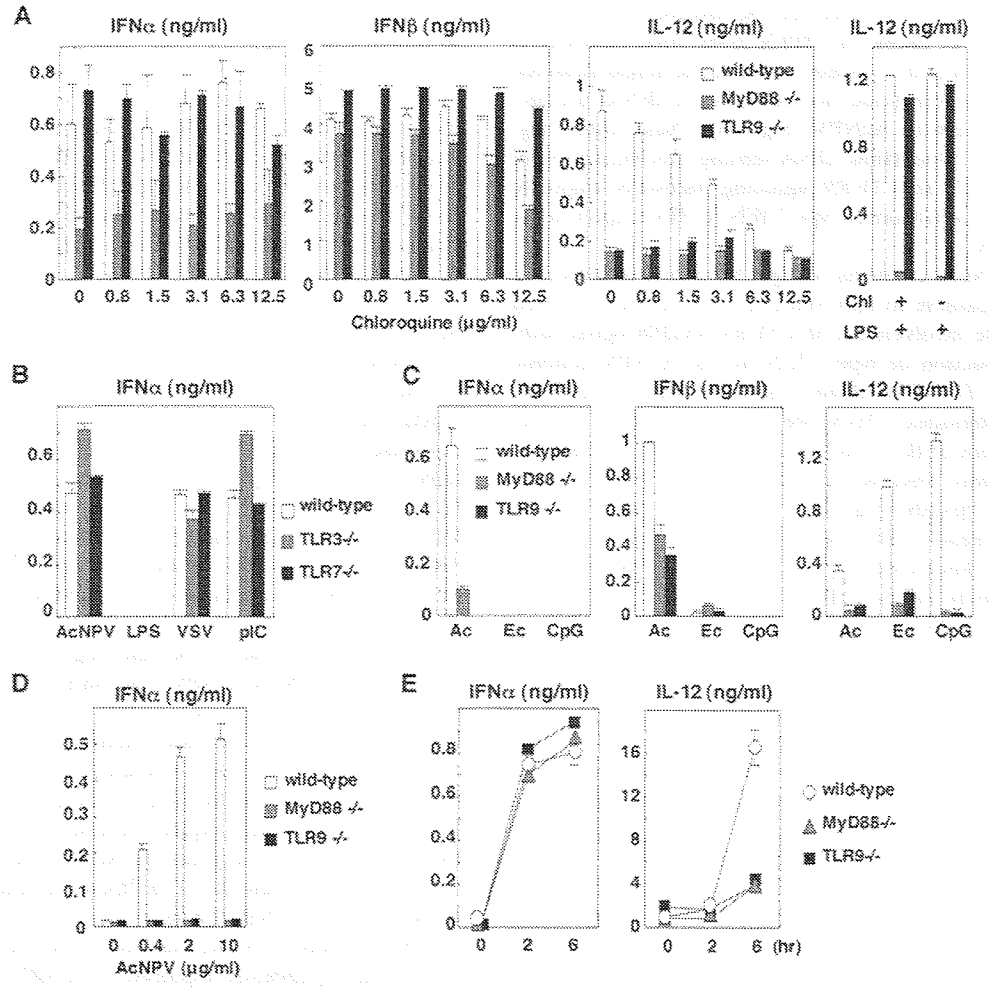

FIG. 1. Involvement of the TLR pathway in the production of type I IFN by AcNPV in immune cells and in mice. (A) PECs (2×10^5 cells/well) prepared from wild-type, MyD88-deficient, or TLR9-deficient mice were stimulated with AcNPV (10 μg/ml) at the indicated concentrations of chloroquine. These cells were also treated with LPS (10 μg/ml) in the presence (+) or absence (−) of chloroquine (Chl) (12.5 μg/ml) (right). After 24 h of incubation, the production of IFN-α, IFN-β, and IL-12 in culture supernatants was determined by ELISA. (B) PECs (2×10^5 cells/well) prepared from wild-type, TLR3-deficient, or TLR7-deficient mice were stimulated with AcNPV (10 μg/ml), LPS (10 μg/ml), VSV (NCP mutant, MOI of 0.1), or poly(I:C) (pIC) (50 μg/ml). After 24 h of incubation, production of IFN-α in culture supernatants was determined by ELISA. (C) PECs prepared as described for panel A were transfected with AcNPV DNA (Ac) (25 μg/ml), *E. coli* DNA (Ec) (25 μg/ml), or mCpG (CpG) (1 μg/ml). After 24 h of incubation, production of IFN-α, IFN-β, and IL-12 in the culture supernatants was determined by ELISA. (D) Splenic pDCs (2×10^5 cells/well) prepared from wild-type, MyD88-deficient, or TLR9-deficient mice were stimulated with AcNPV (10 μg/ml). After 24 h of incubation, production of IFN-α in the culture supernatants was determined by ELISA. (E) AcNPV (100 μg/mouse) was intraperitoneally inoculated into wild-type, MyD88-deficient, or TLR9-deficient mice, and levels of IFN-α and IL-12 production in sera were determined by ELISA at the indicated time points. Data are shown as the means ± standard deviations.

of producing type I IFN in PECs and splenic $CD11c^+$ DCs through a partially MyD88/TLR9-independent pathway (1). Although many studies of the production of type I IFN upon infection with DNA or RNA viruses have been conducted, the precise mechanisms of IFN production by AcNPV remain unclear. To clarify the mechanisms of induction of type I IFN by AcNPV in more detail, we examined the effect of inhibitors of endosomal maturation on the production of type I IFN by AcNPV in PECs derived from wild-type and MyD88- or TLR9-deficient mice. As shown in Fig. 1A, chloroquine clearly inhibited TLR9- or MyD88-dependent IL-12 production in PECs upon infection with AcNPV in a dose-dependent manner but not in cells from TLR9-deficient mice treated with LPS, probably due to the activation of TLR4 on the plasma membrane.

In contrast, AcNPV produces IFN-α and IFN-β through a TLR9-independent and partially MyD88-dependent pathway in PECs, whereas production of type I IFN by AcNPV in PECs was resistant to chloroquine treatment (Fig. 1A). These results indicate that AcNPV produces proinflammatory cytokines and type I IFN in PECs through a TLR-dependent and a TLR-independent pathway, respectively. Furthermore, AcNPV induces type I IFN in PECs through an endocytosis-independent pathway. AcNPV also produced type I IFN in $CD11c^+$ DCs through a TLR9-independent and partially MyD88-dependent pathway, as seen with the PECs, whereas type I IFN production in $CD11c^+$ DCs by AcNPV was sensitive to chloroquine treatment in a dose-dependent manner (data not shown). The partial impairment of IFN-α production in MyD88-deficient

mice suggests that other TLRs may be involved in IFN production by AcNPV. However, PECs from mice deficient in TLR3 and TLR7, which recognize dsRNA and single-stranded RNA, respectively, exhibited no reduction of IFN-α production upon infection with AcNPV (Fig. 1B). These results suggest that a novel cytoplasmic DNA-sensing mechanism other than TLR3, TLR7, and TLR9 signaling pathways might be involved in the production of type I IFN in PECs upon infection with AcNPV.

Although AcNPV contains a high level of unmethylated CpG DNA comparable to that found in the genomes of *E. coli* and HSV (1), the involvement of a TLR9/MyD88 signal pathway in the production of type I IFN by the AcNPV genome remains unclear. *E. coli* DNA and phosphorothioate-stabilized mCpG oligonucleotides (ODN1668) were capable of producing a large amount of IL-12 in PECs through a TLR9/MyD88-dependent pathway, whereas production of type I IFN was not induced by the ligands (Fig. 1C). Production of IL-12 and IFN-α in PECs transfected with the purified baculoviral DNA was impaired by knockout of the TLR9 or the MyD88 gene, whereas substantial amounts of IFN-β were still produced in PECs derived from MyD88- or TLR9-deficient mice (Fig. 1C). These results suggest that a TLR9/MyD88-independent DNA recognition pathway participates in the production of type I IFN in PECs in response to the AcNPV genome.

pDCs are known as master producers of type I IFN upon virus infection, and IFN production is largely dependent on the TLR signaling pathway (11). IFN-α production in pDCs derived from TLR9- or MyD88-deficient mice was severely impaired in response to AcNPV stimulation (Fig. 1D), suggesting that AcNPV induces IFN-α production in pDCs through a TLR9/MyD88-dependent pathway. Next, to examine the mechanisms of induction of type I IFN by AcNPV in vivo, AcNPV was intraperitoneally inoculated into wild-type and MyD88- or TLR9-deficient mice, and levels of IFN-α and IL-12 production in sera were determined. TLR9- or MyD88-deficient mice exhibited a level of serum IFN-α similar to that of wild-type mice upon infection with AcNPV, whereas IL-12 production in the deficient mice was severely impaired (Fig. 1E). These results suggest that non-pDCs participate in the production of type I IFN through a TLR9/MyD88-independent pathway in response to AcNPV in vivo, in contrast to the TLR9/MyD88-dependent production of proinflammatory cytokines. Collectively, these results indicate that both TLR-dependent and -independent pathways are involved in the production of type I IFN in immune cells, including PECs, $CD11c^+$ DCs, and pDCs, in response to AcNPV.

IRF7 plays a crucial role in the production of type I IFN by AcNPV in immune cells and in mice. Both IRF3 and IRF7 are required for the production of type I IFN through a classical pathway activated by viral infection (18, 41). Therefore, we examined the involvement of IRF3 and IRF7 in the production of type I IFN in response to AcNPV by using PECs and splenic $CD11c^+$ DCs derived from IRF3- and IRF7-deficient mice (Fig. 2A). IFN-α production in the IRF7-deficient PECs and splenic $CD11c^+$ DCs in response to AcNPV or VSV was impaired, whereas such production was still active in the IRF3-deficient immune cells. IFN-β production in PECs was impaired in the IRF3- or IRF7-deficient mice in response to AcNPV, although significant amounts of IFN-β were produced in the IRF3- or IRF7-deficient PECs upon infection with VSV. In contrast to the PECs, IRF3-deficient splenic $CD11c^+$ DCs produced a level of IFN-β comparable to that in the wild-type cells in response to AcNPV. In response to VSV infection, production of IFN-β in the deficient immune cells was less impaired. Although enhancement of IL-12 production in the IRF3-deficient PECs and splenic $CD11c^+$ DCs in response to AcNPV or VSV was observed, similar levels of IL-12 production were observed in the IRF7-deficient immune cells and in wild-type cells in response to AcNPV or VSV.

There is circumstantial evidence that IRF7 plays a role in the MyD88-dependent production of IFN-α by activating the TLR in pDCs (17, 25). Therefore, we next examined the IFN-α production in pDCs obtained from IRF7-deficient mice. Consistent with the previous observations, IFN-α production in response to AcNPV was completely abolished in the IRF7-deficient pDCs (Fig. 2B). Furthermore, production of IFN-α, but not that of IL-12 and IL-6, in response to AcNPV in IRF7-deficient mice was severely impaired (Fig. 2C). These results suggest that IRF7 plays a crucial role in the production of type I IFN upon infection with AcNPV in the immune cells and in vivo.

Involvement of the IFNR signaling pathway in the production of type I IFN by AcNPV. The many subtypes of IFN-α and IFN-β are released from infected cells and bind to a single IFNR, and receptor-mediated signal transduction induces the expression of numerous IFN-stimulated genes whose products interfere with viral replication. To determine the involvement of the IFNR-mediated signal transduction in the induction of the innate immune response by AcNPV infection, production of IFN-α, IFN-β, and IL-12 in PECs and splenic $CD11c^+$ DCs derived from IFNR-deficient mice after stimulation with AcNPV or poly(I:C) was examined. Production of IFN-α and IFN-β was significantly impaired by AcNPV or poly(I:C) in the IFNR-deficient PECs and splenic $CD11c^+$ DCs (Fig. 3A and B), whereas IL-12 production in the deficient immune cells was comparable to that in the wild-type cells. In contrast to the in vitro data, production of IFN-α in the sera of IFNR-deficient mice was still detectable and exhibited a partial impairment at 6 h posttreatment (Fig. 3C). These results suggest that production of type I IFN in vitro in response to AcNPV is regulated mainly by an IFNR-mediated signal pathway, whereas an IFNR-independent pathway is additionally involved in the production of type I IFN in response to AcNPV in vivo.

Envelope glycoprotein gp64 does not participate in the immune activation by AcNPV. A previous study demonstrated that the recombinant envelope glycoprotein of AcNPV lacking a transmembrane domain (gp64ΔTM) did not produce proinflammatory cytokines or type I IFN in a murine macrophage cell line, RAW264.7 (1). However, the ability of gp64ΔTM to induce an innate immune response in primary mouse immune cells and nonimmune cells has not yet been examined. To determine the involvement of the envelope glycoprotein of AcNPV in immune activation, we prepared a C-terminally six-His-tagged gp64 lacking the transmembrane region (His-gp64ΔTM), as described previously (1), and examined its ability to activate primary mouse cells, such as PECs, splenic $CD11c^+$ DCs, and MEFs. His-gp64ΔTM was purified as a homogeneous band and was clearly detected by anti-His and anti-gp64 antibodies (Fig. 4A). Although infection with

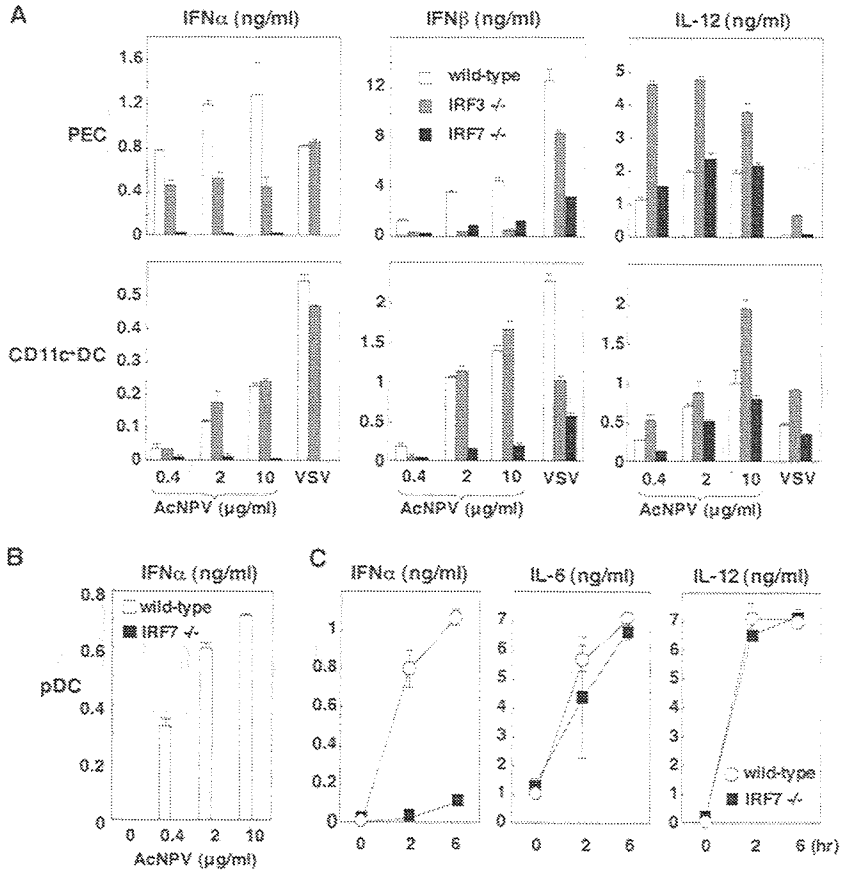

FIG. 2. IRF7 plays a crucial role in the production of type I IFN by AcNPV in immune cells and in mice. (A) PECs and splenic CD11c$^+$ DCs (2×10^5 cells/well) prepared from wild-type, IRF3-deficient, or IRF7-deficient mice were stimulated with the indicated amounts of AcNPV or VSV (NCP mutant, MOI of 0.1). After 24 h of incubation, the production of IFN-α, IFN-β, and IL-12 in culture supernatants was determined by ELISA. (B) Splenic pDCs (2×10^5 cells/well) prepared from wild-type or IRF7-deficient mice were stimulated with the indicated amounts of AcNPV. After 24 h of incubation, production of IFN-α in culture supernatants was determined by ELISA. (C) AcNPV (100 μg/mouse) was intraperitoneally inoculated into wild-type and IRF7-deficient mice, and levels of IL-12, IL-6, and IFN-α production in sera were determined by ELISA at the indicated times. Data are shown as the means ± standard deviations.

AcNPV produced large amounts of IL-12 and IFN-α in PECs and splenic CD11c$^+$ DCs, only a low level of IL-12 production was detected after infection with His-gp64ΔTM (Fig. 4B). Furthermore, infection with AcNPV resulted in rapid production of IFN-β, inflammatory cytokines, and chemokines, including IL-6, MCP-1, RANTES, and IP-10, in MEFs, in contrast to the low level of production of the cytokines by infection with His-gp64ΔTM (Fig. 4C). These results suggest that the envelope glycoprotein, gp64, does not play an important role in the immune activation by AcNPV.

AcNPV produces IFN-β and IFN-inducible chemokines through a TLR-independent and IRF3-dependent pathway in MEFs. We next examined the involvement of the TLR signaling pathway in immune activation by AcNPV in MEFs. MEFs were isolated from wild-type and MyD88/TRIF double knockout mice, and the production of cytokines after stimulation with AcNPV, VSV, LPS, or poly(I:C) was determined by ELISA and real-time PCR. In the MyD88/TRIF-deficient MEFs, the production of IL-6 was severely impaired in response to AcNPV and LPS, whereas no effect was observed after treatment with VSV or poly(I:C) (Fig. 5A, top). In contrast, the production of IFN-β in MEFs in response to AcNPV, VSV, or poly(I:C) was not affected by knockout of the MyD88/TRIF genes. LPS did not induce IFN-β production in either wild-type or MyD88/TRIF-deficient MEFs (Fig. 5A, bottom). Comparable levels of mRNA of IFN-β and IFN-inducible chemokines, including MCP-1, RANTES, and IP-10, were detected in wild-type and MyD88/TRIF knockout MEFs in response to AcNPV (Fig. 5B). These results suggest that a TLR-dependent pathway participates in the production of proinflammatory cytokines by AcNPV in MEFs, as seen with the immune cells, while AcNPV produces IFN-β and IFN-inducible chemokines in MEFs through a TLR-independent pathway.

Next, to determine the involvement of IRF3 and IRF7 in the immune activation in MEFs by AcNPV, wild-type and IRF3- or IRF7-deficient MEFs were treated with AcNPV, LPS, or VSV, and the production of cytokines was determined by ELISA and real-time PCR. Production of IL-6 in IRF3 or IRF7 knockout MEFs after treatment with AcNPV, VSV, or LPS was comparable to that in wild-type MEFs (Fig. 5C, top). In contrast, production of IFN-β was impaired in IRF3- and IRF7-deficient MEFs in response to AcNPV and VSV, respectively, while LPS induced no IFN production in either type of

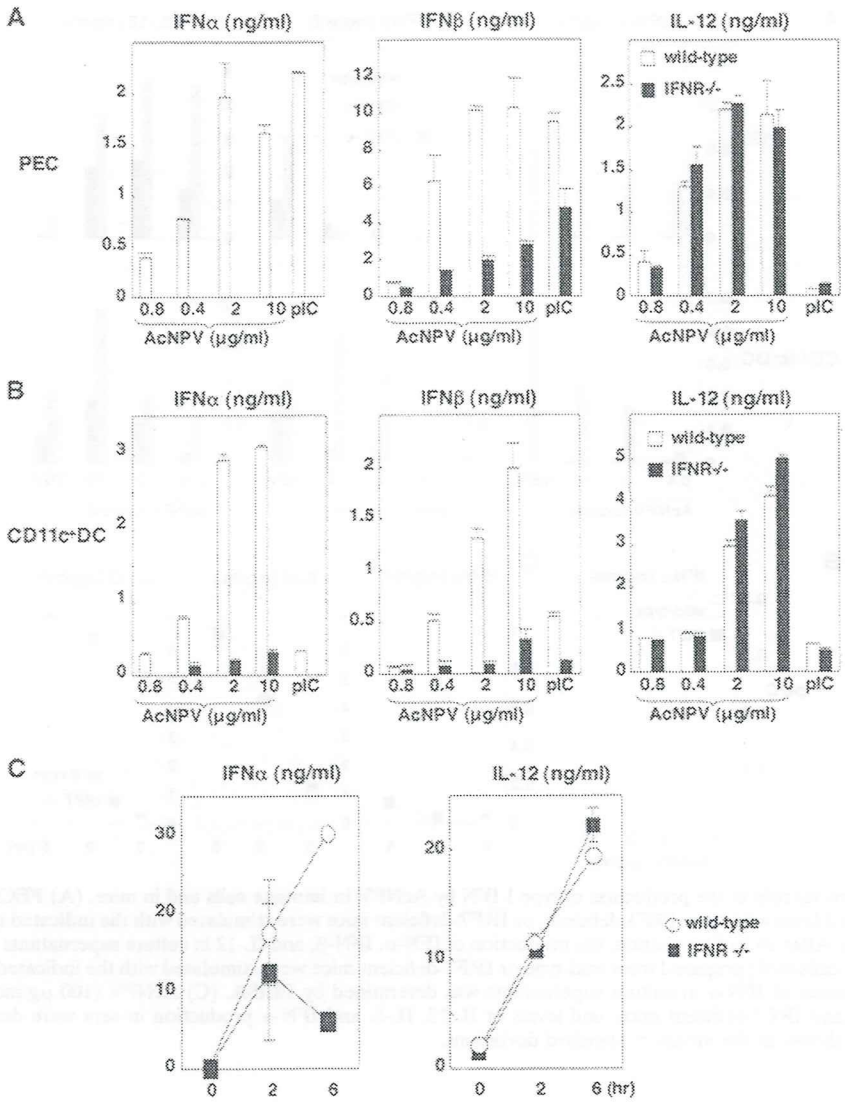

FIG. 3. Involvement of the IFNR signaling pathway in the production of type I IFN by AcNPV. (A and B) PECs (A) and splenic CD11c$^+$ DCs (B) (2×10^5 cells/well) prepared from wild-type and IFNR-deficient mice were stimulated with the indicated amounts of AcNPV or poly(I:C) (pIC) (50 μg/ml). After 24 h of incubation, the production of IFN-α, IFN-β, or IL-12 in culture supernatants was determined by ELISA. (C) AcNPV (100 μg/mouse) was intraperitoneally inoculated into wild-type and IFNR-deficient mice, and levels of IFN-α and IL-12 production in sera were determined by ELISA at the indicated time points. Data are shown as the means ± standard deviations.

MEF (Fig. 5C, bottom). Although robust transcription of IFN-β and IFN-inducible chemokines in response to AcNPV was detected in wild-type and IRF7-deficient MEFs, transcription of the genes in response to AcNPV was severely impaired in IRF3-deficient MEFs (Fig. 5D). These results indicate that AcNPV induces the production of IFN-β and IFN-inducible chemokines through a TLR-independent and IRF3-dependent pathway in MEFs, in contrast to the TLR-dependent and IRF3/IRF7-independent production of IL-6.

AcNPV induces antiviral status in MEFs through an IRF3-dependent pathway. To further examine the involvement of IRF3 in the induction of antiviral status in MEFs in response to AcNPV, wild-type and IRF3-deficient MEFs were transfected with the baculoviral DNA, and the mRNAs of the cytokines were measured. Transcription of IFN-β, IFN-α1, MCP-1, RANTES, and IP-10, but not that of IL-6, was impaired in IRF3-deficient MEFs upon transfection with baculoviral DNA (Fig. 6A).

To determine the involvement of endosomal maturation in the immune activation by AcNPV, the effect of chloroquine on the production of IFN-β and IL-6 in response to AcNPV or LPS was examined. Pretreatment with chloroquine reduced the secretion of IFN-β and IL-6 in MEFs in a dose-dependent manner in response to AcNPV infection but exhibited no effect on IL-6 production in MEFs by LPS treatment (Fig. 6B), suggesting that the impairment of IFN-β and IL-6 production was not due to the cytotoxicity of chloroquine. These results indicate that endosomal maturation is required for the induction of the innate immune response by AcNPV in MEFs.

Next, to determine the antiviral effects of the immune acti-